Key word
233

プラセボ効果

placebo effects

はじめに

「プラセボ」とは，包装，味，におい，感触，形，色および大きさ等の，外観上では実薬との識別が不可能で，薬理活性をもたないもののことである．「プラセボ効果」は，治療効果にかかわらず治療を受けていることに対する正の反応，つまり好ましい反応を意味する．プラセボ効果とは逆に負の反応については，「ノセボ効果（nocebo effect）」という造語が用いられることもある．手術に対するプラセボは基本的には存在しないため，主に薬剤に限定される．

臨床試験におけるプラセボの役割は薬効評価のための対照と盲検化である．プラセボ対照比較試験では，プラセボ群を対照として，被験薬とプラセボ群の効果の差（effect size）を検討し，被験薬の有効性および安全性が推定される．近年は薬効評価を目的とした臨床試験の成績からも，プラセボ反応性自体に関するエビデンスも蓄積されつつある．また医療者が日常診療でプラセボを使用したことのある割合が高いことは複数で報告されており，プラセボ効果は身近な問題である．本項では臨床試験におけるプラセボの諸問題とエビデンスを取り上げ，日常診療での留意点について解説する．

臨床試験におけるプラセボとその効果

プラセボを使用することの倫理性

臨床試験におけるプラセボの使用に関する倫理性はヘルシンキ宣言が基本となり，確立された治療方法が存在しない場合や対象となる治療方法の有効性および安全性を検討するために科学的に必要な場合での使用に制限される．新薬の有効性および安全性を検討する治験等においては有効性および安全性を科学的に証明することが重要であることはいうまでもない．ICH（International Conference on Harmonisation of Technical Requirements for Registration of Pharmaceuticals for Human Use；日米EU医薬品規制調和国際会議）E10ガイドライン[1]では，うつ病や不安障害（原文では「anxiety」）はプラセボに対する反応性が一定しないことが説明されており，そして，厚生労働省や欧州医薬品審査庁（European Medicines Agency : EMEA）が取りまとめた精神疾患領域の臨床試験ガイドライン[2-4]でもプラセボ対照比較試験の必要性が具体的に説明されている．

プラセボ反応性に関するエビデンス

プラセボ反応性は精神疾患ごとに異なり，特にうつ病や不安障害等ではプラセボ反応性が高いことが知られている（図1）．これらの疾患領域の臨床試験では高いプラセボ反応性がeffect sizeに影響し，プラセボに対する優越性を示すことは容易ではないことも報告[6]されており，その大きさは無視できないものである．

一般的に，プラセボ効果は心理学的影響ととらえられがちであるが，神経疾患，心血管機能，呼吸器機能，消化器機能，免疫機能や内分泌機能等の広範な身体機能への影響も認められること[7]から，その効果は心理学的影響にとどまらない．つまり，プラセボ効果には，臨床試験や治療環境下

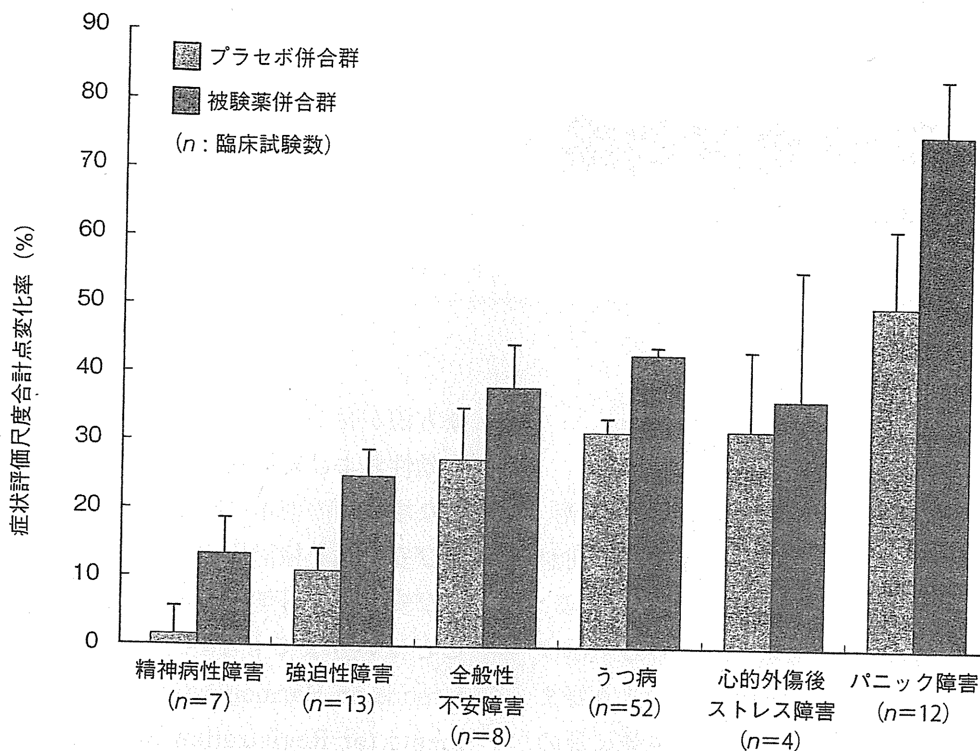

図 1　疾患領域ごとのプラセボと被験薬の反応性

(Khan A, et al. *Psychol Med* 2005[5])

に入ったことで患者自身が食事や睡眠などの生活習慣を改善すること等の影響も含まれ[8]，その機序は明確になっておらず，患者ごとに異なるもので単純ではない．また，プラセボ反応性は個々の患者において異なり，これを識別する方法に乏しいだけでなく，同一の患者においてもその反応性が変化することも知られている[8]．そして，抗うつ薬と薬効が期待できない少量の薬物を陽性プラセボとして投与された臨床試験のメタ解析では，抗うつ薬と陽性プラセボの間での効果の差はきわめて小さいことが示されており[9]，実際はプラセボ効果の程度をとらえることが困難な場合があることを示唆している．

プラセボ反応性に関するエビデンスの日常診療への応用

精神疾患領域の日常診療においても，薬物療法の直接的な効果のほかに，治療に対する知識，社会心理学的要因や生活習慣等が影響することはいうまでもない．プラセボに関するエビデンスは，精神疾患領域のプラセボ対照比較試験の投与期間が 6 ～ 8 週間[2-4]であることが多く，短期的効果に限定されることなど，エビデンスとしての限界はあるが，前述したエビデンスからも臨床においては以下の点を考慮する必要があると思われる．

・社会心理学的影響や環境的要因等の薬物以外の影響の程度は各精神疾患ごとに異なることを考慮して，病態を評価する必要がある．

・薬物療法以外の影響の程度を評価することは困難なこともあるが，種々の要因が影響することもふまえて，特に治療が奏効しない場合では，病態としてのさまざまな可能性について検討する必要がある．

・以上の評価をもとに，薬物療法と非薬物療法のバランスを含む治療戦略を検討する必要がある．

まとめ

プラセボ効果は身近な問題であるが，その特徴

や機序は単純ではない．うつ病や統合失調症等の精神疾患領域の治療の中心は薬物療法であるが，プラセボ反応性に関するエビデンスからも，日常診療においては個々の患者の病態を適切に評価し治療戦略を決定していく必要があると考える．

（中林哲夫）

文献

1) 厚生省医薬局審査課長．「臨床試験における対照群の選択とそれに関連する諸問題」について．医薬審発第136号，平成13年2月27日．
2) 厚生労働省医薬食品局審査管理課長．「抗うつ薬の臨床評価方法に関するガイドライン」について．薬食審査発1116第1号，平成22年11月16日．
3) European Medicines Agency. Note for Guidance on Clinical Investigation of Medical Products in the Treatment of Depression. Doc. Ref. CPMP/EWP/518/97, Rev. 1 : 2002. available online at http://www.ema.europa.eu/pdfs/human/ewp/051897en.pdf
4) European Medicines Agency. Clinical Investigation of Medicinal Products in the Treatment of Schizophrenia. Doc. Ref. CPMP/EWP/559/95, 1998. available online at http://www.ema.europa.eu/pdfs/human/ewp/055995en.pdf
5) Khan A, et al. Magnitude of placebo response and drug-placebo differences across psychiatric disorders. *Psychol Med* 2005 ; 35 : 743–749.
6) Finniss DG, et al. Biological, clinical, and ethical advances of placebo effects. *Lancet* 2010 ; 375 : 686–695.
7) Benedetti F. Placebo Effect. Understanding the Mechanisms Health and Disease. Oxford : Oxford University Press ; 2009.
8) Laughren TP. The scientific and ethical basis for placebo-controlled trials in depression and schizophrenia : An FDA perspective. *Eur Psychiatry* 2001 ; 16 : 418–423.
9) Moncrieff J, Wessely S, Hardy R. Active placebos versus antidepressants for depression. *Cochrane Database Syst Rev* 2004 ; (1) : CD003012.

LETTER

doi:10.1038/nature10456

Pathogenic exon-trapping by SVA retrotransposon and rescue in Fukuyama muscular dystrophy

Mariko Taniguchi-Ikeda[1,2]*, Kazuhiro Kobayashi[1]*, Motoi Kanagawa[1], Chih-chieh Yu[1], Kouhei Mori[1], Tetsuya Oda[1], Atsushi Kuga[1], Hiroki Kurahashi[3], Hasan O. Akman[4], Salvatore DiMauro[4], Ryuji Kaji[5], Toshifumi Yokota[6], Shin'ichi Takeda[7] & Tatsushi Toda[1]

Fukuyama muscular dystrophy (FCMD; MIM253800), one of the most common autosomal recessive disorders in Japan, was the first human disease found to result from ancestral insertion of a SINE-VNTR-*Alu* (SVA) retrotransposon into a causative gene[1–3]. In FCMD, the SVA insertion occurs in the 3′ untranslated region (UTR) of the *fukutin* gene. The pathogenic mechanism for FCMD is unknown, and no effective clinical treatments exist. Here we show that aberrant messenger RNA (mRNA) splicing, induced by SVA exon-trapping, underlies the molecular pathogenesis of FCMD. Quantitative mRNA analysis pinpointed a region that was missing from transcripts in patients with FCMD. This region spans part of the 3′ end of the fukutin coding region, a proximal part of the 3′ UTR and the SVA insertion. Correspondingly, *fukutin* mRNA transcripts in patients with FCMD and SVA knock-in model mice were shorter than the expected length. Sequence analysis revealed an abnormal splicing event, provoked by a strong acceptor site in SVA and a rare alternative donor site in *fukutin* exon 10. The resulting product truncates the fukutin carboxy (C) terminus and adds 129 amino acids encoded by the SVA. Introduction of antisense oligonucleotides (AONs) targeting the splice acceptor, the predicted exonic splicing enhancer and the intronic splicing enhancer prevented pathogenic exon-trapping by SVA in cells of patients with FCMD and model mice, rescuing normal *fukutin* mRNA expression and protein production. AON treatment also restored fukutin functions, including *O*-glycosylation of α-dystroglycan (α-DG) and laminin binding by α-DG. Moreover, we observe exon-trapping in other SVA insertions associated with disease (hypercholesterolemia[4], neutral lipid storage disease[5]) and human-specific SVA insertion in a novel gene. Thus, although splicing into SVA is known[6–8], we have discovered in human disease a role for SVA-mediated exon-trapping and demonstrated the promise of splicing modulation therapy as the first radical clinical treatment for FCMD and other SVA-mediated diseases.

FCMD (incidence 1/34,000 births) shares phenotypic similarities with other severe muscular dystrophies, including muscle–eye–brain disease and Walker–Warburg syndrome. All show deficiencies in *O*-glycosylation of α-DG, an extracellular protein anchored on the plasma membrane. Insufficient *O*-glycosylation interferes with the ability of α-DG to interact with extracellular matrix proteins such as laminin[9,10]. For this reason, FCMD, muscle–eye–brain disease and Walker–Warburg syndrome are categorized as 'α-dystroglycanopathies (α-DGpathy)'[10]; so far, no effective treatments exist for these conditions. SVA is a hominid-specific, composite non-coding retrotransposon that contains SINE (short interspersed sequence), VNTR (variable number of tandem repeat), and *Alu* sequences. It is still active in humans, polymorphic and mobilized by the human LINE-1 *in trans*[6,11–15].

In previous work, we showed that *fukutin* mRNA (10 exons, 7.4- and 6.4-kilobase (kb) cDNAs in size with two poly-A sites, 461-amino-acid protein with calculated molecular mass of 53.7 kDa) was not detectable by northern blot analysis in patients with FCMD carrying the SVA insertion[2]. To investigate the aetiology of this decreased expression, we have now analysed whole *fukutin* mRNA in lymphoblasts from patients with FCMD using quantitative PCR with reverse transcription (qRT–PCR). PCR products corresponding to the protein-coding region of *fukutin*, as well as those including sequences in the distal part of the 3′ UTR (and thus downstream of the SVA insertion), were similar in abundance to those from an unaffected control (Fig. 1a). However, products located at sequence positions within the 3′ UTR were markedly decreased relative to the control. From these results and along with previous reports of many 3′ and 5′ splice sites within SVA elements[6–8], we hypothesized that abnormal splicing occurs somewhere between the end of the fukutin protein-coding region and the SVA insertion.

We then performed long-range RT–PCR using primers that flank the region corresponding to decreased expression. In patients with FCMD, we detected a single 3-kb PCR product, which is shorter than the 5-kb product seen in the normal control (Fig. 1b). This observation was consistent in several tissue types from patients with FCMD (Supplementary Fig. 1). PCR from genomic DNA produced an 8-kb product in patients with FCMD, compared with a 5-kb product in the control (Fig. 1b). Sequence analysis of the 3-kb product from FCMD cDNA revealed a splicing event (Supplementary Fig. 2). This event generates a new donor-side breakpoint within the final coding exon (exon 10), located 116 base pairs (bp) upstream from the authentic stop codon. A rare alternative donor site at that position is activated and trapped by an alternative acceptor site located within the inserted SVA, creating an additional and aberrant exonic sequence (exon 11) (Fig. 1c). The acceptor-side breakpoint is located 274 bp downstream from the start of the SVA insertion, between ag and TC (Fig. 1c). The acceptor site has not been described in the previous reports of SVA splicing[6,7]. This location is preceded by a pyrimidine-rich stretch, the SVA $(TCTCCC)_{41}$ hexamer at the 5′ end of the SVA element, with a possible favourable branch point. Predicted exonic splicing enhancer sites occur around 70 bp downstream from the new acceptor site. We confirmed that the aberrant splicing event can be abolished by replacing AG with GG at the acceptor junction in cultured cells transfected with a *fukutin* construct carrying SVA insertion (Supplementary Fig. 3). *Fukutin* expression was not altered by cycloheximide treatment, indicating that the transcript was not subject to nonsense-mediated mRNA decay, possibly because this exon-trapping occurred within the last

[1]Division of Neurology/Molecular Brain Science, Kobe University Graduate School of Medicine, Kobe 650-0017, Japan. [2]Division of General Pediatrics, Kobe University Graduate School of Medicine, Kobe 650-0017, Japan. [3]Division of Molecular Genetics, Institute for Comprehensive Medical Science, Fujita Health University, Aichi 470-1192, Japan. [4]Department of Neurology, Columbia University Medical Center, New York, NY 10032, USA. [5]Department of Clinical Neuroscience, The University of Tokushima Graduate School, Tokushima 770-8503, Japan. [6]Department of Medical Genetics, Faculty of Medicine and Dentistry, University of Alberta, Edmonton, AB T6G 2H7, Canada. [7]Department of Molecular Therapy, National Institute of Neuroscience, National Center of Neurology and Psychiatry, Tokyo 187-8502, Japan.
*These authors contributed equally to this work.

©2011 Macmillan Publishers Limited. All rights reserved

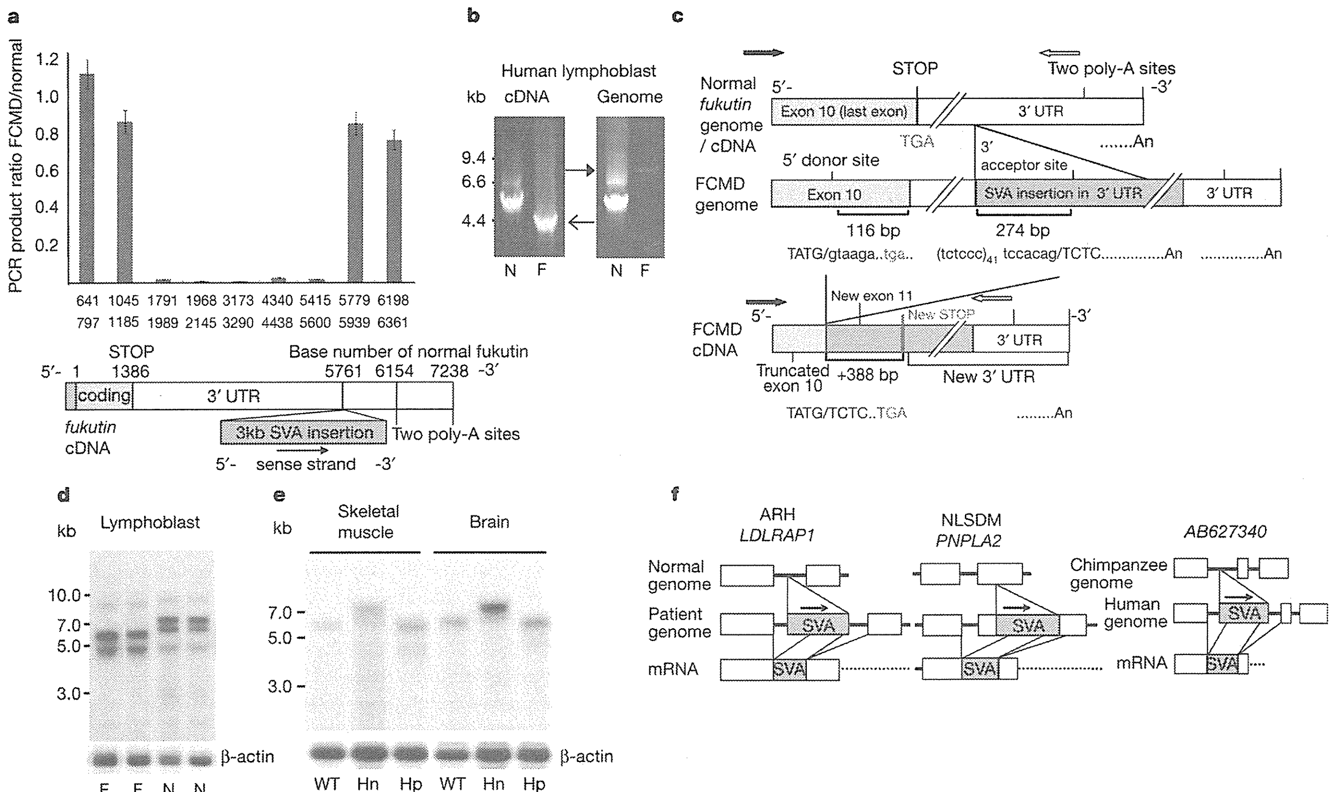

Figure 1 | An SVA retrotransposal insertion induces abnormal splicing in FCMD. **a**, Expression analysis of various regions of *fukutin* mRNA in lymphoblasts. Grey bar, the ratio of RT–PCR product in patients with FCMD relative to the normal control; numbers on the *x* axis, nucleotide positions of both forward and reverse primers in *fukutin*. Error bars, s.e.m. **b**, Long-range PCR using primers flanking the expression-decreasing area (nucleotide position 1,061–5,941) detected a 3-kb PCR product in FCMD lymphoblast cDNA (open arrow) and an 8-kb product in FCMD genomic DNA (filled arrow). In the normal control, cDNA and genomic DNA both showed 5-kb PCR products. The 8-kb band was weak, probably because VNTR region of SVA is GC-rich (82%). **c**, Representation of genomic DNA and cDNA in FCMD. Black and white arrows, forward and reverse sequencing primers. The intronic sequence in FCMD is indicated in lower case. The authentic stop codon is coloured red, and the new stop codon is coloured blue. **d**, **e**, Northern blot analysis of *fukutin* in human lymphoblasts (**d**) and model mice (**e**); F, FCMD; N, normal control. The wild-type mouse *fukutin* mRNA was detected at a size of 6.1 kb. Both skeletal muscle (left) and brain (right) showed smaller, abnormal bands in Hp/Hp mice. WT, wild type; Hn, Hn/Hn mice; Hp, Hp/Hp mice. **f**, Representation of genomic DNA and cDNA in ARH (*LDLRAP1*, left), NLSDM (*PNPLA2*, middle) and human (*AB627340*, right).

exon, and the new stop codon exists downstream of the new last exon–exon junction (Supplementary Fig. 4).

We have recently generated knock-in mice that carry a humanized fukutin exon 10, which either includes (Hp allele) or excludes (Hn allele) the SVA insertion, and bred these strains with heterozygous fukutin knockout mice to obtain compound heterozygotes (Hp/−)[16]. Knock-in mice that are homozygous (Hp/Hp) and compound heterozygous (Hp/−) are representative of the human FCMD alleles. These mice exhibit hypoglycosylation of α-DG in skeletal muscle, which is the most significant characteristic in α-DGpathy[16]. Quantitative RT–PCR in various tissues from Hp/Hp mice revealed an aberrant splicing pattern identical to that seen in human patients (Supplementary Fig. 5). Northern blot analysis detected abnormally spliced *fukutin* mRNA species at the expected sizes of 5.6 and 4.6 kb in patients with FCMD, whereas the normal *fukutin* mRNAs appeared at 7.4 and 6.4 kb (Fig. 1d and Methods). We replicated these results in the knock-in model mice (Fig. 1e and Supplementary Fig. 6a). The consistent observations between patients with FCMD and knock-in model mice lead us to conclude that a splicing abnormality underlies the pathogenesis of FCMD.

Abnormal splicing excises the authentic stop codon and produces another stop codon located 388 bp downstream from the 5′ side of the new exon 11 (Fig. 1c). The predicted protein lacks the C-terminal 38 amino acids of fukutin, instead containing 129 amino acids derived from the SVA sequence (Supplementary Fig. 7). Endogenous fukutin is scarce and difficult to detect; however, we were able to identify both normal and aberrant forms of the protein in human and mouse using immunoprecipitation followed by western blot analysis. The abnormal fukutin protein in FCMD displayed the predicted mobility shift (Fig. 2a–c and Supplementary Fig. 6b).

We introduced normal and aberrantly spliced *fukutin* cDNA constructs into mammalian cell lines. Whereas normal fukutin localized to the Golgi apparatus, the aberrantly spliced fukutin protein is displaced completely from the Golgi to the endoplasmic reticulum (Fig. 2d and Supplementary Fig. 8). Further examination showed that a *fukutin* construct lacking the C-terminal 38 amino acids also mislocalized to the endoplasmic reticulum (Fig. 2d and Supplementary Fig. 8), suggesting that the C-terminal domain of fukutin is important for localization to the Golgi. Thus, impairment of this domain may lead to fukutin dysfunction in FCMD. The mislocalization is unlikely to be toxic because FCMD is an autosomal recessive disease and heterozygous carriers of the SVA insertion have no symptoms.

We next tested if exon-trapping occurs in other diseases with SVA insertion[6]. In a patient with autosomal recessive hypercholesterolemia (ARH), a 2.6-kb SVA was inserted within intron 1 of the *LDLRAP1* gene[4]. A patient with lipid storage disease with subclinical myopathy (NLSDM) also had a 1.9-kb SVA insertion in exon 3 of the *PNPLA2* gene[5]. We found abnormally spliced products induced by SVA exon-trapping in these patients' fibroblast (Fig. 1f left and middle panels, Supplementary Figs 9 and 10, and Supplementary Table 1). Cycloheximide treatment to fibroblasts from these patients increased expression of the genes (Supplementary Figs 9a and 10a), suggesting

©2011 Macmillan Publishers Limited. All rights reserved

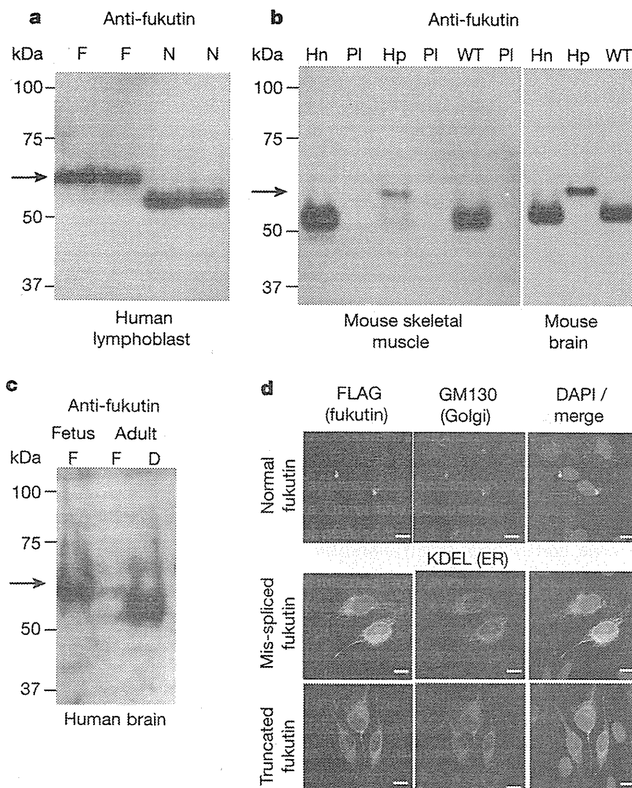

Figure 2 | Abnormal fukutin protein in FCMD. **a–c**, Immunoprecipitation analysis of fukutin protein in human lymphoblasts (**a**), both skeletal muscle and brain tissues from Hp/Hp mice (**b**) and brain tissue from patients with FCMD (**c**); filled arrow, abnormal fukutin; N, normal sample; F, sample from patient with FCMD; Hn, Hn/Hn mice; Hp, Hp/Hp mice; PI, pre-immune serum; D, patient with Duchenne muscular dystrophy. **d**, The subcellular localization of fukutin. Top, normal fukutin; middle, mis-spliced fukutin; bottom, truncated fukutin. Stained with anti-FLAG (left, to detect fukutin), anti-GM130 (middle, Golgi marker, top) and anti-KDEL (endoplasmic reticulum marker, middle and bottom), and merge (right, with DAPI stain). Scale bar, 10 μm.

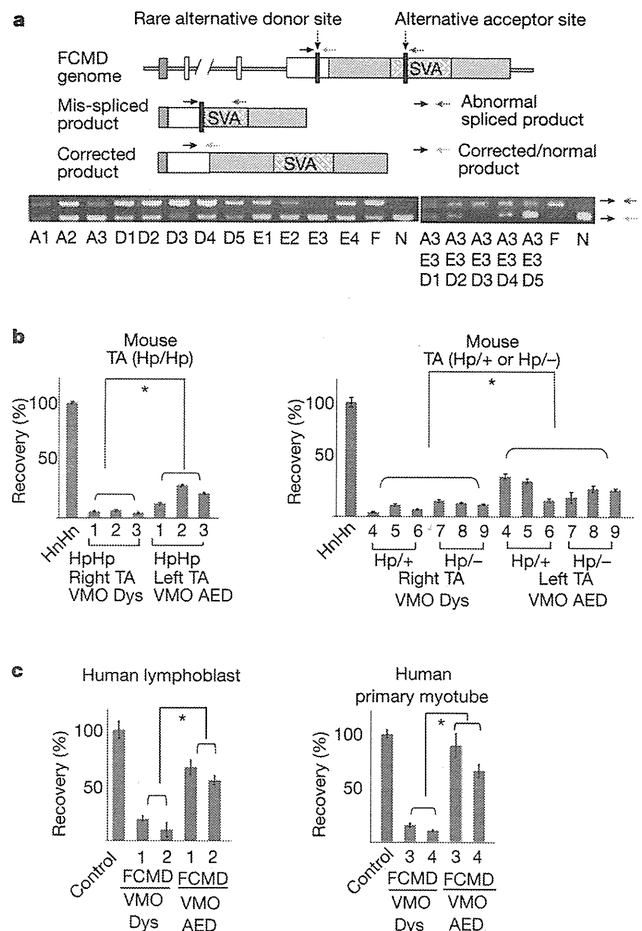

Figure 3 | AON cocktail rescues normal *fukutin* mRNA. **a**, RT–PCR diagram of three primers designed to assess normal *fukutin* mRNA recovery (upper). Black arrow, a common forward primer located on *fukutin* coding region; dark grey arrow, a reverse primer to detect the abnormal RT–PCR product (161 bp); light grey arrow, the other reverse primer to detect the restored normal RT–PCR product (129 bp). The effect on Hp/Hp ES cells treated with each single or a cocktail of AONs (lower). F, FCMD; N, normal sample. **b**, Rescue from abnormal splicing in VMO-treated Hp/Hp and Hp/− mice. Local injection of AED cocktail into tibialis anterior ($n = 3$). Dys, a negative control. **c**, Rescue from abnormal splicing in VMO-treated human FCMD lymphoblasts (left, $n = 2$) and myotubes (right, $n = 2$). The y axis shows the percentage recovery of normal mRNA (*$P < 0.01$ by Student's t-test). TA, tibialis anterior. Error bars, s.e.m.

that the SVA-trapped transcripts are likely to be subjected to nonsense-mediated mRNA decay[6,17]. In a search for the same events using the same acceptor site as FCMD in the human genome, we located two expressed sequence tags on human chromosome 4 (DA436529 and DA060755) that represent a spliced transcript induced by an SVA element. We found exonization in a human-specific insertion of SVA (AB627340) into a small gene (Fig. 1f right panel and Supplementary Fig. 11). The human-specific exon-trapping of SVA in the small gene might influence human evolution and development.

FCMD alleles of the *fukutin* gene contain a fully intact protein coding sequence, raising the possibility that FCMD could be treated by restoring translation of the full-length protein through splicing modulation with AONs. To identify promising target sequences in various cell lines, we produced 25-mer 2′-O-methyl phosphoramidite (2′OMePS) AONs targeted to the acceptor (A1–A3), donor (D1–D5) and exonic splicing enhancer sites (E1–E4) in *fukutin* pre-mRNA (Supplementary Fig. 12). We introduced the AONs into various cell types and assessed the recovery of normal processing and restoration of the authentic stop codon (Fig. 3a). Cells with A3 and E3 showed strong suppression of SVA-derived splicing. The greatest recovery of *fukutin* mRNA, to levels of more than 40% of the normal control, was achieved with a combination of A3, E3 and D5 (AED) (Fig. 3a). The D5 sequence overlaps with a predicted intronic splicing enhancer site within the aberrant intronic sequence; in normal *fukutin*, this sequence resides in exon 10 (Supplementary Fig. 12).

We injected octa-guanidine morpholino oligonucleotide (vivo-morpholino, VMO)[18] AED cocktail locally into skeletal muscle of knock-in mice and evaluated the therapeutic effect by calculating the percentage recovery of normally processed mRNA. In the AED-treated tibialis anterior and gastrocnemius of Hp/Hp and Hp/− mice, the amount of corrected *fukutin* mRNA increased significantly relative to mice treated with control VMO (Fig. 3b and Supplementary Fig. 13). We assessed fukutin protein recovery in injected skeletal muscle tissue from Hp/Hp mice. Consistent with the significant increase of restored normal mRNA, normal fukutin protein was rescued (Fig. 4a). We examined α-DG glycosylation in AED-treated Hp/− mice. Deficiently glycosylated α-DG, at the predicted smaller size, was reduced in abundance, whereas normal-sized α-DG increased after AED treatment (Fig. 4b). The signal intensity for glycosylated α-DG was clearly increased, and a shift in the α-DG core was observed, indicating that the rescued fukutin is functional. Laminin overlay assays revealed a marked increase in α-DG laminin-binding ability, indicating that α-DG

©2011 Macmillan Publishers Limited. All rights reserved

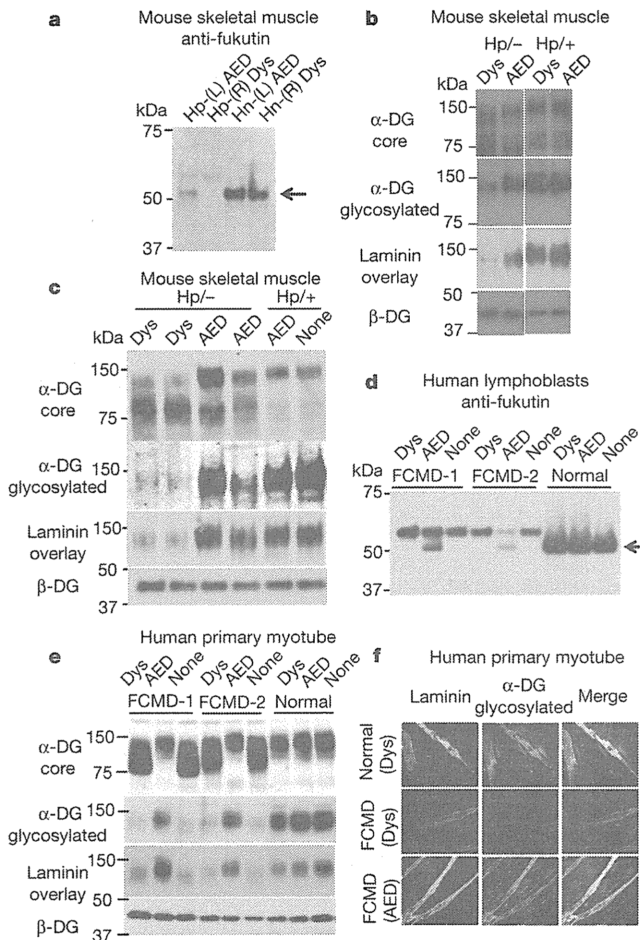

Figure 4 | AON cocktail treatment rescues normal fukutin protein and functional α-DG. a, d, Immunoprecipitation analysis of fukutin protein after local treatment with VMO (AED) in FCMD model mice (**a**) and human FCMD lymphoblasts (**d**). Arrow, normal fukutin protein. L, left tibialis anterior; R, right tibialis anterior; Dys, negative control. **b, c, e,** Tibialis anterior muscle after local (**b**) or systemic (**c**) treatment with AED and human FCMD lymphoblasts treated with the AED (**e**) were analysed by western blot using antibodies against α-DG core protein (top panel) and glycosylated α-DG (second), and by a laminin overlay assay (third). Bottom, β-DG (internal control). **f,** Laminin clustering assay. Left, anti-laminin; middle, anti-glycosylated α-DG; right, merged images. Upper, normal myotubes treated with control VMO; middle, FCMD patient myotubes treated with control VMO; bottom, FCMD patient myotubes treated with AED.

function also is recovered (Fig. 4b). We next tested systemic AED treatment by intravenous injection of Hp/− mice. This treatment also showed the recovery of normally glycosylated α-DG in AED-treated mice (Fig. 4c).

We administered the VMO AED cocktail to human lymphoblasts and myotubes. As in knock-in mice, we observed successful correction of the splicing abnormality. The corrected *fukutin* mRNA was restored to 50% or more of the levels seen in normal controls (Fig. 3c). We believe this to be sufficient recovery, considering that unaffected FCMD carriers have only 50% of normal *fukutin* mRNA. Finally, we tested recovery of the fukutin protein and the glycosylation of α-DG in the cells of patients with FCMD. Not only was normal fukutin protein expression significantly rescued in AED-treated lymphoblasts (Fig. 4d), but also we observed recovery of normally glycosylated α-DG in AED-treated myotubes (Fig. 4e). Immunofluorescence staining also showed immensely increased glycosylated α-DG (Fig. 4f). A laminin clustering assay showed increased laminin clustering ability, which is characteristically absent in α-DGpathy[19] (Fig. 4f). These data show that AED treatment effectively rescues normal fukutin, confirming our observation of abnormal *fukutin* splicing and raising the possibility of splicing modulation therapy as the first treatment for FCMD. To treat neuronal migration disorder of FCMD, prenatal treatment may be necessary, but it is currently difficult for ethical and technical reasons. Nevertheless, improving even only the muscular symptoms would greatly ameliorate quality of life of the patients as well as their families.

Retrotransposons account for nearly half of the human genome[20]. Increased numbers of reports have highlighted positive and negative contributions of retrotransposons to human health and disease[21,22]. In addition to being the causative factor for FCMD, ARH and NLSDM, SVA insertions have also been implicated in hereditary elliptocytosis, X-linked agammaglobulinemia, neurofibromatosis type 2 and X-linked dystonia-Parkinsonism[12,23–26]. It has been suggested that SVA insertions cause such diseases through genomic deletion, reduced mRNA expression or skipping of neighbouring exons[17,22]. Recently, SVA splicing has been suggested to generate variation within and across species by activating functional 3′ splice sites within SVAs across the human genome, controlling gene transcription, creating alternative splicing by exon-trapping, or inducing premature stop codons, and was experimentally demonstrated[6]. Our findings emphasize the importance of SVA functions in human disease and support the possibility of radical treatment against SVA-induced disease by splicing modulation therapy. AONs have become one of the most promising and practical candidate chemicals for splicing modulation therapy in cancer[27], infectious diseases[28] and Duchenne muscular dystrophy[29,30]. In demonstrating the ability of AONs to rescue fukutin function in FCMD, we introduce a novel clinical role for them in treating FCMD and other SVA-mediated diseases, while providing new insights about the influence of SVAs on human evolution, development and disease.

METHODS SUMMARY

For AON treatment, 25-mer 2′OMePS (GeneDesign and Invitrogen) and octa-guanidine morpholino (VMO; Gene-Tools) were used. The knock-in mouse was produced as described previously[16].

Full Methods and any associated references are available in the online version of the paper at www.nature.com/nature.

Received 16 September 2010; accepted 12 August 2011.

1. Toda, T. *et al.* Localization of a gene for Fukuyama type congenital muscular dystrophy to chromosome 9q31–33. *Nature Genet.* **5,** 283–286 (1993).
2. Kobayashi, K. *et al.* An ancient retrotransposal insertion causes Fukuyama-type congenital muscular dystrophy. *Nature* **394,** 388–392 (1998).
3. Watanabe, M. *et al.* Founder SVA retrotransposal insertion in Fukuyama-type congenital muscular dystrophy and its origin in Japanese and Northeast Asian populations. *Am. J. Med. Genet. A.* **138,** 344–348 (2005).
4. Wilund, K. R. *et al.* Molecular mechanisms of autosomal recessive hypercholesterolemia. *Hum. Mol. Genet.* **11,** 3019–3030 (2002).
5. Akman, H. O. *et al.* Neutral lipid storage disease with subclinical myopathy due to a retrotransposal insertion in the *PNPLA2* gene. *Neuromuscul. Disord.* **20,** 397–402 (2010).
6. Hancks, D. C. *et al.* Exon-trapping mediated by the human retrotransposon SVA. *Genome Res.* **19,** 1983–1991 (2009).
7. Damert, A. *et al.* 5′-Transducing SVA retrotransposon groups spread efficiently throughout the human genome. *Genome Res.* **19,** 1992–2008 (2009).
8. Bantysh, O. B. & Buzdin, A. A. Novel family of human transposable elements formed due to fusion of the first exon of gene MAST2 with retrotransposon SVA. *Biochemistry (Mosc.)* **74,** 1393–1399 (2009).
9. Michele, D. E. *et al.* Post-translational disruption of dystroglycan-ligand interactions in congenital muscular dystrophies. *Nature* **418,** 417–422 (2002).
10. Barresi, R. & Campbell, K. P. Dystroglycan: from biosynthesis to pathogenesis of human disease. *J. Cell Sci.* **119,** 199–207 (2006).
11. Strichman-Almashanu, L. Z. *et al.* Retroposed copies of the HMG genes: a window to genome dynamics. *Genome Res.* **13,** 800–812 (2003).
12. Ostertag, E. M. *et al.* SVA elements are nonautonomous retrotransposons that cause disease in humans. *Am. J. Hum. Genet.* **73,** 1444–1451 (2003).
13. Bennett, E. A. *et al.* Natural genetic variation caused by transposable elements in humans. *Genetics* **168,** 933–951 (2004).
14. Wang, H. *et al.* SVA elements: a hominid-specific retroposon family. *J. Mol. Biol.* **354,** 994–1007 (2005).

©2011 Macmillan Publishers Limited. All rights reserved

15. Hancks, D. C. *et al.* Retrotransposition of marked SVA elements by human L1s in cultured cells. *Hum. Mol. Genet.* **20,** 3386–3400 (2011).
16. Kanagawa, M. *et al.* Residual laminin-binding activity and enhanced dystroglycan glycosylation by LARGE in novel model mice to dystroglycanopathy. *Hum. Mol. Genet.* **18,** 621–631 (2009).
17. Hancks, D. C. & Kazazian, H. H. Jr. SVA retrotransposons: evolution and genetic instability. *Semin. Cancer Biol.* **20,** 234–245 (2010).
18. Wu, B. *et al.* Octa-guanidine morpholino restores dystrophin expression in cardiac and skeletal muscles and ameliorates pathology in dystrophic mdx mice. *Mol. Ther.* **17,** 864–871 (2009).
19. Barresi, R. *et al.* LARGE can functionally bypass α-dystroglycan glycosylation defects in distinct congenital muscular dystrophies. *Nature Med.* **10,** 696–703 (2004).
20. Lander, E. S. *et al.* Initial sequencing and analysis of the human genome. *Nature* **409,** 860–921 (2001).
21. Kazazian, H. H. Jr. Mobile elements: drivers of genome evolution. *Science* **303,** 1626–1632 (2004).
22. Cordaux, R. & Batzer, M. A. The impact of retrotransposons on human genome evolution. *Nature Rev. Genet.* **10,** 691–703 (2009).
23. Hassoun, H. *et al.* A novel mobile element inserted in the α spectrin gene: spectrin dayton. A truncated α spectrin associated with hereditary elliptocytosis. *J. Clin. Invest.* **94,** 643–648 (1994).
24. Rohrer, J. *et al.* Unusual mutations in Btk: an insertion, a duplication, an inversion, and four large deletions. *Clin. Immunol.* **90,** 28–37 (1999).
25. Legoix, P. *et al.* Molecular characterization of germline NF2 gene rearrangements. *Genomics* **65,** 62–66 (2000).
26. Makino, S. *et al.* Reduced neuron-specific expression of the TAF1 gene is associated with X-linked dystonia-parkinsonism. *Am. J. Hum. Genet.* **80,** 393–406 (2007).
27. O'Brien, S. *et al.* Randomized phase III trial of fludarabine plus cyclophosphamide with or without oblimersen sodium (Bcl-2 antisense) in patients with relapsed or refractory chronic lymphocytic leukemia. *J. Clin. Oncol.* **25,** 1114–1120 (2007).
28. Crooke, S. T. *et al.* Vitravene—another piece in the mosaic. *Antisense Nucleic Acid Drug Dev.* **8,** vii–viii (1998).
29. Lu, Q. L. *et al.* Functional amounts of dystrophin produced by skipping the mutated exon in the mdx dystrophic mouse. *Nature Med.* **9,** 1009–1014 (2003).
30. Alter, J. *et al.* Systemic delivery of morpholino oligonucleotide restores dystrophin expression bodywide and improves dystrophic pathology. *Nature Med.* **12,** 175–177 (2006).

Supplementary Information is linked to the online version of the paper at www.nature.com/nature.

Acknowledgements We thank S. Nakagawa, K. Ohno, S. Tsujino, N. Taniguchi, and I. Nonaka for comments; M. Okabe and A. Kawai for generating the ES cell line from knock-in model mice; Y. Motoyoshi and J. C. Cohen for providing patients' samples; W. Sako and Y. Izumi for sending patients' samples; I. Mizuta, T. Mure, M. Furukawa, K. Kaneshiro, Y. Dainin and all laboratory members for technical support; and J. Logan for editing the manuscript. We thank the GAIN for providing chimpanzee brain samples. This work was supported by an Intramural Research Grant (20B-13) for Neurological and Psychiatric Disorders from the National Center of Neurology and Psychiatry (to T.T.), the Global COE Program (Frontier Biomedical Science Underlying Organelle Network Biology) (to T.T., M.T.-I. and M.K.) from the Ministry of Education, Culture, Sports, Science and Technology of Japan, Grants-in-Aid for Scientific Research (A) (23249049 to T.T.), and Young Scientists (A) (21689030 to K.K.) and (B) (20790980 to M.T.-I.) from the Japan Society for the Promotion of Science, and the Takeda Science Foundation (to K.K.).

Author Contributions M.T.-I., K.K., M.K. and T.T. designed the study. M.T.-I. performed most of the experiments. K.K. developed a system to detect endogenous fukutin protein. M.K. performed biochemical analysis of VMO-injected mice. C.Y. produced the *fukutin* cDNA constructs for transfection experiments. K.M., T.O., and A.K. performed analyses of AON treatment in mice and various cell types. H.K., T.Y. and S.T. provided intellectual input. H.O.A., S.D. and R.K., provided patients' samples. M.T.-I., K.K. and T.T. wrote the paper.

Author Information The patient *fukutin* and a chimpanzee mRNA sequences are deposited in GenBank/European Molecular Biology Laboratory/DNA Data Bank of Japan under accession numbers AB609007 and AB627340, respectively. Reprints and permissions information is available at www.nature.com/reprints. The authors declare no competing financial interests. Readers are welcome to comment on the online version of this article at www.nature.com/nature. Correspondence and requests for materials should be addressed to T.T. (toda@med.kobe-u.ac.jp).

©2011 Macmillan Publishers Limited. All rights reserved

METHODS

Antisense oligonucleotides. Twenty-five-mer 2′OMePS (GeneDesign and Invitrogen) and VMO oligonucleotides (Gene-Tools) were designed to target potential splice-modulating sequences of SVA-inserted *fukutin*, including a splicing acceptor site, a splicing donor site, exonic splicing enhancers and intronic splicing enhancers as follows: A1, CCGTGGAAGGAGACTGTGGAGGGAG; A2, GGAGACCGTGGAAGGAGACTGTGGA; A3, AGAGGGAGACCGTGGA AGGAGACTG; E1, CACCGTCCAGCCTTGGCTCGGCATC; E2, CTGCAGTG AGCCGAGATGGCAGCAG; E3, GAGGCAGGAGAATCAGGCAGGGAGG; E4, GAAAACCAGTGAGGCGTAGCAGGCT; D1, CAGGTCTTACCATAGT TGGCTTCAA; D2, CAGGAATCTTCCAGGTCTTACCATA; D3, GAGCGCTT CCAGTCCCACGTCTTTA; D4, TCCATTGGGTTGCACATTGGGAGGA; D5, CATCCCACTCAGAAATAGGCCAGAT; DYS, GGCCAAACCTCGGCTTAC CTGAAAT[31]. U (uracil) was used instead of T (thymine) for the synthesis of 2′O-MePS oligonucleotides. Target sequences are shown in Supplementary Fig. 12. Exonic splicing enhancer sites were predicted by ESEfinder 3.0 (http://rulai.cshl.edu/cgi-bin/tools/ESE3/esefinder.cgi), and intronic splicing enhancer sites were predicted by ACESCAN2 (http://genes.mit.edu/acescan2/index.html). AONs were solubilized in sterile distilled water.

Animals and cells. All mouse experimental protocols were approved by the Ethics Review Committees for Animal Experimentation at Osaka University Graduate School of Medicine and Kobe University Graduate School of Medicine. FCMD knock-in model mice and the mouse nomenclature have been described previously[16]. The transgenic alleles containing normal and SVA-inserted human exon 10 were named Hn and Hp, respectively: Hp/Hp is homozygous for the SVA allele; Hn/Hn is homozygous for the normal allele; Hp/+ and Hp/− are SVA carriers and compound heterozygotes for the SVA and knockout alleles, respectively. The ages of mice used in experiments varied from 2 to 6 months. The mouse ES cell line carrying the SVA-inserted human genomic *fukutin* exon 10 was generated from Hp/Hp mice. The ES cell line carrying a *fukutin* knockout allele has been described previously[32]. The commercially available mouse ES cell line AB2.2 was used as a control. Human lymphoblasts were obtained from patients with FCMD with homozygous SVA insertions and from unaffected individuals. Human primary myoblasts were derived from muscle biopsies from patients with FCMD and unaffected individuals. Human primary fibroblasts were obtained by skin biopsy from patients with ARH and NLSDM. Human autopsy brain samples were obtained from patients with FCMD (fetus and 34-year-old) and DMD (34-year-old). Chimpanzee brain sample was provided by the Great Ape Information Network, Japan. Human brain RNA was purchased from Clontech. All clinical samples were used with the approval of Human Ethics Review Committees of Osaka University Graduate School of Medicine and Kobe University Graduate School of Medicine.

Myoblast differentiation. Myoblast cells were maintained at 37 °C and 5% CO_2 in DMEM medium plus 20% fetal bovine serum, 2.5 ng ml^{-1} of basic fibroblast growth factor (Sigma), and a 0.5% penicillin–streptomycin–amphotericinB mix (Wako). Myotubes were obtained from confluent myoblast cultures after 10–14 days of serum deprivation and replacement with 2% FBS.

RNA isolation, RT–PCR, qRT–PCR and sequencing. To inhibit nonsense-mediated mRNA decay, cycloheximide (100 μg ml^{-1}) (Sigma) was added to the culture medium 24 h before RNA isolation. For RT–PCR and qRT–PCR, total RNA was extracted using the RNeasy Plus Mini kit (Qiagen), and cDNA was obtained using the Superscript III One-step RT–PCR system (Invitrogen) with random primers, following the manufacturer's instructions. SYBR Pre-mix Ex Taq (Takara) was used for qRT–PCR, and expression values were normalized to *gapdh* as an internal control for mRNA quantity. Data were obtained from triplicate experiments. To detect abnormally spliced RT–PCR products from patients with FCMD, ARH and NLSDM, and from human brain *AB627340* cDNA, long-range PCR was performed using LA Taq with LA Taq Buffer II (Takara), adding dimethyl sulphoxide and 7-deaza-dGTP (Roche). The RT–PCR products were directly sequenced (FCMD and NLSDM), or cloned with the TOPO TA Cloning Kit (Invitrogen) before sequencing (ARH and AB627340). To calculate the expression ratio in Fig. 1a and Supplementary Figs 4, 5, 9, 10 and 13, the value in the mutant sample was divided by the value in the normal sample, as measured by qRT–PCR. To identify AON target sequences, we designed three primers to distinguish recovered transcripts from unrecovered transcripts by AON treatment (Fig. 3a). Similarly, we designed three primers to compare expression amount of SVA-trapped to SVA-untrapped transcripts of the *AB627340* gene (Supplementary Fig. 11a). One primer on SVA in Fig. 3a and Supplementary Fig. 11a was within *Alu*-like domain: the sequence was 5′-GAAAACCAGTGAGGCGTAGC-3′. To calculate the percentage recovery of normal mRNA processing in Fig. 3b, c and Supplementary Fig. 13, the value of treated sample was divided by that of normal samples, as measured by qRT–PCR at sequence position 1341, where the authentic stop codon resides. Primer sequences for qRT–PCR and RT–PCR are available upon request.

Northern blot analysis. Previous attempts to detect *fukutin* mRNA in patients with FCMD by northern blot analysis have been unsuccessful[2], probably because the predicted mRNA sequence is the same size as abundant ribosomal RNA. Moreover, the tertiary structure of *fukutin* mRNA is presumably complicated owing to the immensely GC-rich SVA sequence. Therefore, we performed northern blot analysis of FCMD and control mRNA after treatment to remove abundant ribosomal RNA and strong denaturation to untangle the *fukutin* transcript. Total RNA (1 mg) was extracted from human lymphoblasts, mouse ES cells, mouse brain and mouse skeletal muscle using TRIzol (Invitrogen). Oligotex-dT30<Super> (Takara) was used to extract more than 3 μg of poly-A RNA. Ribosomal RNA was removed using Ribo-Minus (Invitrogen). Stronger denaturation of RNA was achieved by incubating polyA-RNA samples with a combination of 0.8 M glyoxal and 50% DMSO in 10 mM sodium phosphate buffer (pH 7.0) for 60 min at 55 °C. Three micrograms of poly-A RNA was loaded on the agarose gel. A *fukutin* cDNA clone covering the fukutin coding sequence was ^{32}P-labelled and used as a probe.

cDNA expression constructs. The normal fukutin cDNA encodes full-length fukutin protein. The spliced fukutin construct encodes abnormal fukutin, as shown in Supplementary Fig. 7. The truncated fukutin construct lacks the C-terminal 38 amino acids. All constructs encoded FLAG epitope tags fused to the C terminus of the expressed protein.

Cell transfection. HeLa S3 cells and C2C12 cells were transfected with normal fukutin construct, spliced fukutin construct and truncated fukutin construct using FuGENE 6 (Roche). Fukutin localization was determined using immunocytochemistry 2 days after transfection. For transfection of AONs, 2′OMePS were introduced into various cell lines, including mouse ES cells, human myoblasts and human lymphoblasts, using Lipofectin (Invitrogen).

Detection of endogenous fukutin protein. The polyclonal rabbit anti-fukutin antibody RY213 recognizes the peptide CLKIESKDPRLDGIDS, and the polyclonal goat-anti-fukutin antibody 106G2 recognizes full-length fukutin protein lacking the amino (N)-terminal hydrophobic domain. Endogenous fukutin was detected by immunoprecipitation using 106G2, from cell or tissue lysates containing 5–10 mg of total protein in lysis buffer (1% Nonidet P-40, 0.5% deoxycholate, 0.1% SDS, 20 mM Tris-Cl, pH 7.5 and 150 mM NaCl), followed by western blot analysis using affinity-purified RY213.

Immunofluorescence and western blot analysis. Cells were washed and fixed with 4% paraformaldehyde in PBS. The following primary antibodies were used: anti-GM130 (monoclonal, BD Bioscience), anti-KDEL (monoclonal, Stressgen), anti-FLAG (rabbit polyclonal, MBL), anti-α-DG (monoclonal, IIH6C4 and VIA4-1, Millipore) and anti-laminin (rabbit polyclonal, Sigma). To stain nuclei, 4′6-diamidino-2-phenylindole (DAPI, Sigma) was added to the secondary antibody solution at a final concentration of 1 ng ml^{-1}. Cells were observed under fluorescence confocal microscopy (Carl Zeiss). Western blot analysis and laminin overlay assays were performed as described previously[16].

Mutagenesis analysis. We made the four *fukutin* constructs: pHn, human normal *fukutin* construct consisting of exon 2–9 cDNA and genomic normal exon 10; pHp, patient *fukutin* construct consisting of exon 2–9 cDNA and genomic patient exon 10 with SVA insertion; pSpl, patient *fukutin* construct pHp, which lacks the abnormally spliced region; pAcc, patient *fukutin* construct pHp with AG to GG replacement at the acceptor site within the SVA sequence. These constructs were transfected into HeLa S3 cells using Effectene (Qiagen). After extraction of poly-A RNA by Oligotex, northern blot analysis was performed using 2 μg of poly-A RNA for each sample with stronger denaturation mentioned above.

AON treatment of FCMD model mice. For intramuscular injection, we injected cardiotoxin (10 μM) (Latoxan) percutaneously into tibialis anterior (0.3 nmol) and gastrocnemius (0.7 nmol) of Hp/+, Hp/−, Hp/Hp and Hn/Hn mice on day 0 ($n = 3$ for each genotype). On days 1, 4 and 7, VMO (400 mg kg^{-1}) solubilized in sterile distilled water was injected. AED and Dys were administered to the left and the right legs, respectively. For systemic injection, an intraperitoneal injection of butorphanol tartrate (5 mg kg^{-1}) (Bristol-Myers Squibb) was performed on day 0. VMO (20 mg kg^{-1}) solubilized in 5% glucose solution was administered by intravenous injection through the tail vein on days 1 and 7 ($n = 4$ for Hp/−, $n = 2$ for Hp/+). Mice were killed on day 21, and total RNA or protein lysate was isolated from each tissue for further analyses of *fukutin* mRNA expression, fukutin protein translation, and glycosylation of α-DG.

AON treatment of human patient cell lines. For protein analysis, VMO cocktails (AED and Dys) were introduced into FCMD and normal control lymphoblasts at a final concentration of 2.5 μM in culture medium using a Gene Pulser II Electroporator (0.25-kV voltage, 960-μF capacitance, with 0.4-cm gene pulser cuvettes, giving a time-constant readout of approximately 40 ms) (Bio-Rad) ($n = 2$). For glycosylation analysis, VMO cocktails (AED and Dys) were introduced into myoblasts from patients with FCMD and normal control cells by direct

©2011 Macmillan Publishers Limited. All rights reserved

addition to the culture medium at a final concentration of 4 μM ($n = 2$). After incubation for 48 h, cells were collected and total RNA or protein lysate was isolated.

Laminin clustering assay. The AED cocktail was introduced into myotubes by direct addition to the culture medium at a total concentration of 4 μM after a medium change on day 2. On days 10–14, mouse EHS laminin-1 (Sigma) was added with fresh medium at a concentration of 1.0 nM and incubated for 30 min, followed by immunocytochemistry.

SVA sequence analysis. SVA sequence was aligned to the SVA reference sequence present in Repbase (http://www.girinst.org/repbase/update/index.html)[33] and the location on the SVA reference of the splicing acceptor and donor sites in SVA was determined.

31. Yokota, T. *et al.* Efficacy of systemic morpholino exon-skipping in Duchenne dystrophy dogs. *Ann. Neurol.* **65,** 667–676 (2009).
32. Takeda, S. *et al.* Fukutin is required for maintenance of muscle integrity, cortical histiogenesis and normal eye development. *Hum. Mol. Genet.* **12,** 1449–1459 (2003).
33. Jurka, J. Repbase Update: a database and an electronic journal of repetitive elements. *Trends Genet.* **9,** 418–420 (2000).

©2011 Macmillan Publishers Limited. All rights reserved

Takano et al. BMC Cardiovascular Disorders 2011, 11:23
http://www.biomedcentral.com/1471-2261/11/23

BMC
Cardiovascular Disorders

RESEARCH ARTICLE | Open Access

Assessment of left ventricular regional function in affected and carrier dogs with duchenne muscular dystrophy using speckle tracking echocardiography

Hiroshi Takano[1], Yoko Fujii[1*], Naoko Yugeta[1,2], Shinichi Takeda[2] and Yoshito Wakao[1]

Abstract

Background: Two-dimensional speckle tracking echocardiography (STE) is a relatively new method to detect regional myocardial dysfunction. To assess left ventricular (LV) regional myocardial dysfunction using STE in Duchenne muscular dystrophy model dogs ($CXMD_J$) without overt clinical signs of heart failure.

Methods: Six affected dogs, 8 carrier dogs with $CXMD_J$, and 8 control dogs were used. Conventional echocardiography, systolic and diastolic function by Doppler echocardiography, tissue Doppler imaging (TDI), and strain indices using STE, were assessed and compared among the 3 groups.

Results: Significant differences were seen in body weight, transmitral E wave and E' wave derived from TDI among the 3 groups. Although no significant difference was observed in any global strain indices, in segmental analysis, the peak radial strain rate during early diastole in posterior segment at chordae the tendineae level showed significant differences among the 3 groups.

Conclusions: The myocardial strain rate by STE served to detect the impaired cardiac diastolic function in $CXMD_J$ without any obvious LV dilation or clinical signs. The radial strain rate may be a useful parameter to detect early myocardial impairment in $CXMD_J$.

Background

Duchenne progressive muscular dystrophy (DMD) is characterized by progressive degeneration of skeletal and cardiac muscles with fibrotic tissue replacement and fatty infiltration [1]. Resulting myocardial dysfunction has been estimated to be responsible for death in 20% of human DMD patients [2,3].

Echocardiography is one of the useful noninvasive methods used to assess cardiac function in patients and animals with Duchenne's cardiomyopathy [4-9]. It is possible that the recognition of earlier subclinical cardiac systolic or diastolic dysfunction could allow for an early medical approach, thus improving long-term cardiovascular outcomes. Several studies have demonstrated the usefulness of tissue Doppler imaging (TDI) to detect subclinical myocardial systolic and diastolic dysfunction in patients with normal conventional echocardiographic parameters [10]. These studies have also confirmed that myocardial velocities, myocardial wall-thickening velocities, myocardial velocity gradients and strain during systole and early diastole in the left ventricular free wall were reduced in patients [11-15] and dogs with DMD [16,17]. However, strain measurements derived from TDI involve several disadvantages including angle-dependence and the limitations of an available cardiac region for an assessment. Since it has been reported that the distribution of myocardial lesions detected by magnetic resonance imaging (MRI) and single photon emission computed tomography (SPECT) varied among DMD patients [18-20], TDI might underestimate the severity of myocardial dysfunction in certain patients.

Two-dimensional speckle tracking echocardiography (STE) is a new approach designed to assess left ventricular function in humans and animals [21,22]. STE has no angle-dependence and allows the assessment of any region of the heart. Usefulness of STE analysis in human patients with idiopathic dilated cardiomyopathy to detect systolic and diastolic dysfunction has been described in

* Correspondence: fujiiy@azabu-u.ac.jp
[1]Department of Surgery 1, School of Veterinary Medicine, Azabu University, Kanagawa, Japan
Full list of author information is available at the end of the article

BioMed Central
© 2011 Takano et al; licensee BioMed Central Ltd. This is an Open Access article distributed under the terms of the Creative Commons Attribution License (http://creativecommons.org/licenses/by/2.0), which permits unrestricted use, distribution, and reproduction in any medium, provided the original work is properly cited.

several reports. STE provides several advantages over TDI, in for example, estimation for the increase in LV filling pressure [23-25]. In addition, STE has the ability to detect regional myocardial dysfunction [22]. We hypothesized that STE could detect early myocardial lesions in patients with Duchenne's cardiomyopathy without clinical signs. To our knowledge, there have been no reports assessing the cardiac function of Duchenne's cardiomyopathy using STE.

Canine X-linked muscular dystrophy in Japan ($CXMD_J$) is a Beagle-based dog colony established by artificially inseminating frozen semen from spontaneous Golden retriever muscular dystrophy. $CXMD_J$ has been reported to be comparable to human patients and dogs with DMD [9,26-28]. The purpose of the present study was to assess left ventricular regional myocardial dysfunction using STE in affected and carrier $CXMD_J$ dogs without overt clinical signs of heart failure.

Methods

Animals

Beagles aged 8 months old or more from a $CXMD_J$ colony at the Division of Laboratory Animal Resources, National Institute of Neuroscience, National Center of Neurology and Psychiatry used in the present study included 6 dogs affected with $CXMD_J$, 8 carrier dogs, and 8 control dogs. Control dogs had no history of cardiopulmonary diseases, and each had a normal physical examination, standard 6 lead electrocardiogram and conventional echocardiogram. Dogs were categorized as affected, carrier or normal (control) dogs on the basis of DNA analysis conducted immediately after the birth [27]. All experiments were approved by the Ethics Committee for the Treatment of Laboratory Animals of the National Institute of Neuroscience (approval No. 20-03 and 21-03).

Echocardiographic Examination

All echocardiographic images were acquired using Vivid S6 (GE Medical System, Tokyo, Japan) ultrasound unit equipped with a 7 MHz transducer and were obtained by one trained examiner (HT). Dogs were restrained manually in lateral recumbency. Skilled experimental animal technicians handled the dogs and assisted in the experiments. For dogs that became agitated, the examination was performed 15 minutes after sedation with acepromazine (0.01 mg/kg, IV, A.C.P. 10, 10 mg/mL, Delvet, The State of New South Wales, Australia) and buprenorphine (0.0075 mg/kg, IV, Lepetan injection, 0.2 mg/mL, Otsuka, Tokyo, Japan). ECG monitoring with clear R wave recognition was recorded in concurrence with an echocardiographic examination using the same ultrasound unit. The mean value of variables in 3 consecutive cardiac cycles was used for statistical analysis.

Conventional Echocardiography

M-mode echocardiographic measurements were made from the right parasternal short-axis view at the chordae tendineae (Ct) level (LV end-diastolic and end-systolic internal diameters [LVIDd and LVIDs], and fractional shortening [FS]). We calculated left ventricular end-diastolic volume (EDV), left ventricular end-systolic volume (ESV) and left ventricular ejection fraction (EF) from LV internal diameters using the Teichholz method. LV end-diastolic and end-systolic volume indices (EDVI and ESVI) were derived from EDV and ESV divided by body surface area (BSA), respectively [29]. Diameters of the left atrium (LAD) and aortic root (AoD) were measured from the right parasternal short-axis view at the heart base level by B-mode method, and the LA/Ao ratio was calculated [30].

Systolic and Diastolic Function by Doppler Echocardiography and TDI

Systolic time intervals (pre-ejection period [PEP] and LV ejection time [ET]) were measured using an aortic flow velocity curve [31]. Transmitral inflows (TMF) were created from the left parasternal apical 4-chamber view. Early (E wave) and late (A wave) filling velocities, the E wave deceleration time (DcT) and E/A ratio were measured from the transmitral flow tracing. Left ventricular isovolumic relaxation time (IVRT) was calculated as the time difference between the intervals from the beginning of the Q wave on the ECG to the onset of early diastolic flow and intervals from the Q wave to the end of aortic flow tracing. Tissue Doppler trace of mitral annulus velocity (MAV) on the lateral side was obtained from the left parasternal apical 4-chamber view to measure peak velocities during systole (S') and during early diastole (E'). Then, the E/E' was calculated [32,33].

Speckle Tracking Echocardiography (STE)

Right parasternal short-axis views at Ct level were used to measure all STE indices below, because myocardial lesion of dogs with $CXMD_J$ was reported to be localized in free wall at basal level of LV [9]. Images were acquired in cine loops triggered by the QRS complex, saved in digital format, and analyzed using off-line software (EchoPAC PC '08 [a]). The principal of speckle tracking analysis has been described in several previous studies [21,22,34-37]. All analysis was performed by one observer (HT).

For the each of 6 regions of interest, peak systolic radial and circumferential strains (SR and SC), and peak radial and circumferential strain rates during systole and early diastole (SrR_S, SrR_E, SrC_S and SrC_E) were measured at the level of the Ct (Figure 1). The E/SrR_E and E/SrC_E were derived from E divided by SrR_E and SrC_E, respectively. Since the values of radial and circumferential

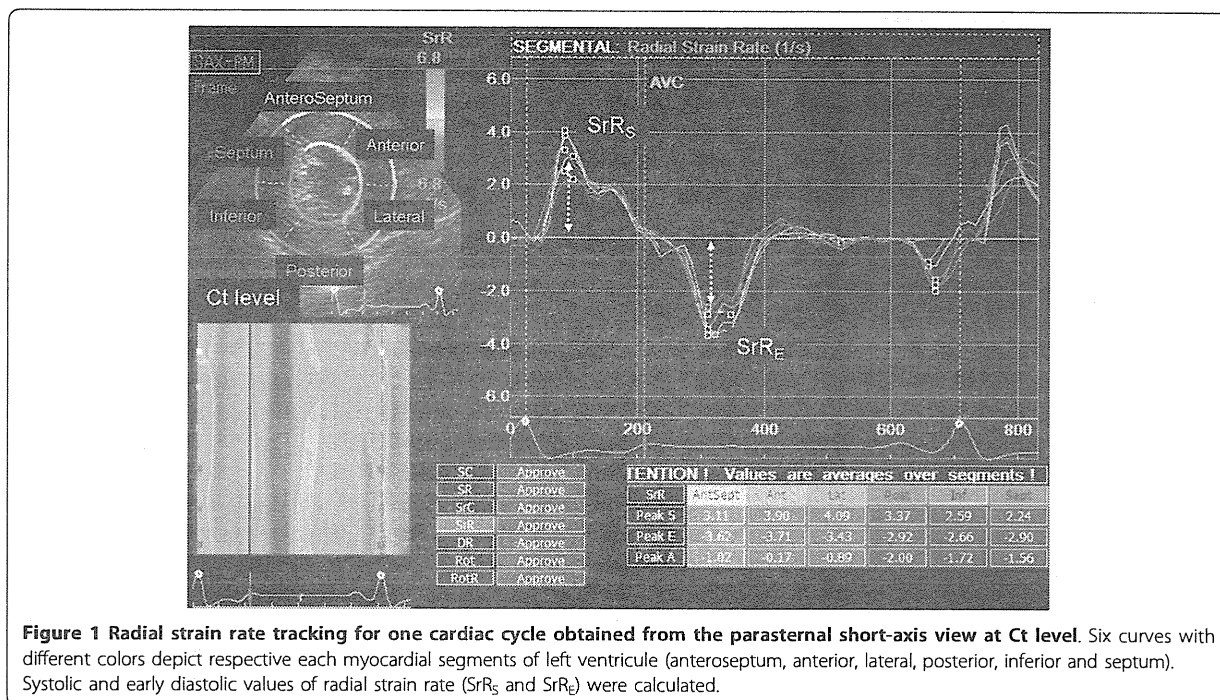

Figure 1 Radial strain rate tracking for one cardiac cycle obtained from the parasternal short-axis view at Ct level. Six curves with different colors depict respective each myocardial segments of left ventricule (anteroseptum, anterior, lateral, posterior, inferior and septum). Systolic and early diastolic values of radial strain rate (SrR_S and SrR_E) were calculated.

direction were calculated from 6 segments as described previously, the mean of all 6 segments and the mean of each segmental value were calculated for all parameters.

Experimental Protocols

Conventional echocardiographic parameters, systolic time intervals, diastolic functional parameters and STE indices were obtained and compared among the affected, carrier and normal dogs.

Since sedatives were administered when a dog was not cooperative, the influence of sedation on all indices was assessed using 6 normal dogs. Parameters were obtained at baseline and 15 minutes after sedation with acepromazine (0.01 mg/kg, IV) and buprenorphine (0.0075 mg/kg, IV), and then compared.

For the assessment of reproducibility, intraobsever variability of STE analysis was assessed by use of images from 6 normal dogs. Using same cine loops, each STE value was determined again 3 weeks after the primary analysis.

Statistics

Comparisons among the 3 groups were performed using one-way ANOVA. A post hoc testing for the difference among the groups was performed by the Steel method. The assessment of the influence of sedation was performed using the paired *t*-test. When the normality test failed, the Wilcoxon signed-rank test was applied. Intraobserver variability was express as mean of absolute difference as the percentage of the mean of two absolute measurements. A value of $P < 0.05$ was considered statistically significant.

Results

Animals

The characteristics of affected, carrier and normal dogs in the present study are shown in Table 1. There was a significant difference in BW among the 3 groups.

Influence of Sedation

A significant difference between pre- and post-sedation values was seen in HR and ESVI. In addition, a significant difference was also seen in the A wave of TMF (Table 2).

Conventional Echocardiography

No significant difference among the 3 groups was noted in any parameters (Table 3). Mild mitral regurgitation (MR) was detected using the color Doppler imaging in 1 carrier dog.

Systolic and Diastolic Function by Doppler Echocardiography (Table 4)

Significant differences were seen in E wave of TMF and MAV on the lateral side (E') among the 3 groups.

Speckle Tracking Echocardiography

The frame rate used for this study to analyze STE indices ranged from 72 to 93 frames per second. Frames

Table 1 Characteristics of each group

Index	Unit	Normal dogs	Carrier dogs	Affected dogs
Number		8	8	6
Gender	F/M	4/4	8/0	3/3
Number of sedated dogs		5	6	4
Age	months	32.86 ± 29.73	33.13 ± 23.68	24.50 ± 15.27
Body weight	kg	12.19 ± 1.04	11.41 ± 1.22	9.49 ± 2.05†

†: Significant difference compared with normal dogs by multiple comparison ($P < 0.05$).

per cardiac cycle were 57.38 ± 6.53, 49.36 ± 10.70 and 49.44 ± 12.16 frames, in normal, carrier and affected dogs, respectively, and there was no significant difference among the 3 groups ($P = 0.21$). Intraobserver variability of measurements was 3.6 to 13.2%. Table 5 shows the results of global values in the STE indices of the 3 groups. In strain indices, only E/SrR_E had significant differences between normal and carrier dogs.

SrR_E in the posterior segments were significantly decreased in carrier and affected dogs when segmental values were compared with normal dogs (Figure 2 and table 6).

Discussion

In the present study, no significant difference was found in any parameters using conventional echocardiography among the 3 groups, which indicated no apparent LV dilation or systolic dysfunction with normal FS in affected and carrier dogs.

SrR_E has been reported to show a significant correlation with LV relaxation [38,39]. A significant difference in SrR_E was observed in posterior segments at the Ct level in carrier and affected dogs. SrR_E tended to decrease in other LV segments. The results of segmental STE analysis suggest an impairment of LV relaxation in the basal inferoposterior segments of $CXMD_J$ - affected dogs prior to a detectable decrease in global indices of cardiac function. In previous studies, pathological lesions were frequently observed in the posterior and lateral wall of the left ventricle in patients and dogs with DMD [9,40,41]. Previous reports have indicated that TDI-derived parameters also identified myocardial dysfunction in the LV free wall [11,14-17,42], which supported our results.

Circumferential strain parameters in affected dogs were not significantly changed in the present study. In contrast, Mertens et al. reported significant decreases in TDI-derived strain indices in the apical, mid and basal level of LV long-axis views in DMD patients [15]. One possible explanation for this difference is more advanced disease in the previously reported population, supported by the presence of obvious LV dilation in the patients of that study. A second possibility is different measurement techniques. Mizuguchi et al. have suggested that LV systolic dysfunction may begin with reduced longitudinal shortening that is compensated by augmented circumferential shortening in early stages. Therefore, one could hypothesize that STE performed using long-axis views is a more sensitive method than with short-axis views, although it was not evaluated in the present study.

E wave velocity in carrier dogs was significantly increased compared with normal dogs. Increased E wave was noticed in dogs with overt and occult dilated cardiomyopathy (DCM), which may suggest diastolic dysfunction [43]. However, in the present study, the other measured parameters derived from transmitral flow, such as DcT and A wave velocity, were all within the reference range and no statistical significance was found among groups. In addition, the TMF pattern was not the typical restrictive pattern (i.e. E/A>2 as well as short DcT) in any individual carrier dogs [43,44]. The clinical relevance of this finding is uncertain given the relatively small magnitude of difference and the large amount of overlap in values among groups. In addition, higher value of E/SrR_E in carrier dogs might be influenced by the increased E wave. E' measured using TDI was significantly reduced in affected dogs compared with normal dogs. This is similar to a previous report of reduced peak E' velocity in patients with DMD [13].

Duchenne's cardiomyopathy in a carrier female was previously reported, though it was found to be mild compared with that in an affected male [45,46]. In the present study, there was significant difference in segmental assessment of SrR_E between normal and carrier female dogs as well as affected dogs. Since our carrier females

Table 2 Effects of sedation on echocardiographic parameters

Index		Unit	Awake	Sedated	*P* value
Conventional echocardiography	HR	bpm	89.10 ± 27.29	69.61 ± 7.01	< 0.05
	ESVI	mL/m^2	27.37 ± 3.64	21.43 ± 3.61	0.0042
Transmitral flow	A wave	cm/sec	46.33 ± 12.41	34.22 ± 8.28	0.015

ESVI = Left ventricular end-systolic index; A = Peak velocity of late diastolic flow in transmitral flow (results with P value < 0.05).

Table 3 Conventional echocardiographic parameters of each group

Index	Unit	Normal dogs	Carrier dogs	Affected dogs
HR	bpm	92.54 ± 11.22	106.39 ± 26.22	102.16 ± 35.79
EF	%	65.42 ± 8.13	67.13 ± 10.35	62.89 ± 13.05
FS	%	35.04 ± 6.66	36.92 ± 8.41	33.61 ± 9.87
EDVI	mL/m^2	59.19 ± 19.53	69.79 ± 20.62	53.35 ± 27.03
ESVI	mL/m^2	15.43 ± 4.57	20.04 ± 11.02	17.87 ± 13.75
LA/Ao		1.22 ± 0.095	1.17 ± 0.14	1.08 ± 0.081

EF = Ejection fraction; FS = Fractional shortening; EVDI = Left ventricular end-diastolic index; ESVI = Left ventricular end-systolic index; LA/Ao = Left atrial diameter/aortic root diameter ratio.

Table 4 Echocardiographic systolic and diastolic parameters using Doppler of each group

Index		Unit	Normal dogs	Carrier dogs	Affected dogs
Systolic time intervals	PEP/ET		0.21 ± 0.037	0.21 ± 0.046	0.22 ± 0.085
Transmitral flow	E wave	cm/sec	74.71 ± 13.42	87.42 ± 10.89†	66.44 ± 10.19
	A wave	cm/sec	45.79 ± 14.68	45.71 ± 8.09	44.61 ± 8.98
	E/A		1.82 ± 0.71	1.98 ± 0.44	1.58 ± 0.52
	DcT	msec	92.29 ± 8.20	91.54 ± 14.44	91.06 ± 14.73
Isovolumic relaxation time		msec	32.13 ± 11.49	28.21 ± 10.07	39.28 ± 13.61
Mitral annular velocity	S' wave	cm/sec	10.67 ± 1.60	12.17 ± 5.94	7.39 ± 1.25
	E' wave	cm/sec	12.13 ± 2.62	11.33 ± 2.12	8.67 ± 1.65†
	E/E'		6.39 ± 1.57	7.89 ± 1.41	8.48 ± 2.17

†: Significant difference compared with normal dogs by multiple comparison ($P < 0.05$).

PEP = Pre-ejection period; ET = Left ventricular ejection time; E = Peak velocity of early diastolic flow in transmitral flow; A = Peak velocity of late diastolic flow in transmitral flow; DcT = Deceleration time of early diastolic flow; S'= Peak mitral annular velocity during systole; E'= Peak mitral annular velocity during early diastole.

Table 5 STE indices of each group

Index		Unit	Normal dogs	Carrier dogs	Affected dogs
Radial	SR	%	44.50 ± 9.63	49.58 ± 14.76	46.68 ± 12.63
	SrR_S	/sec	2.71 ± 0.41	2.82 ± 0.68	2.78 ± 0.63
	SrR_E	/sec	-3.06 ± 0.50	-2.55 ± 0.73	-2.23 ± 0.95
	E/SrR_E		-24.81 ± 5.21	-36.20 ± 8.73†	-34.24 ± 12.88
Circumferential	SC	%	-20.87 ± 3.86	-22.76 ± 5.14	-23.04 ± 5.38
	SrC_S	/sec	-2.49 ± 0.26	-2.77 ± 0.72	-3.04 ± 0.86
	SrC_E	/sec	2.84 ± 0.61	2.92 ± 0.78	2.70 ± 0.49
	E/SrC_E		27.15 ± 7.08	31.80 ± 8.92	25.50 ± 6.48

†: Significant difference compared with normal dogs by multiple comparison ($P < 0.05$).

SR = peak systolic radial strain; SrR_S = Peak radial strain rate during systole; SrR_E = Peak radial strain rate during early diastole; SC = Peak systolic circumferential strain; SrC_S = Peak circumferential strain rate during systole; SrC_E = Peak circumferential strain rate during early diastole.

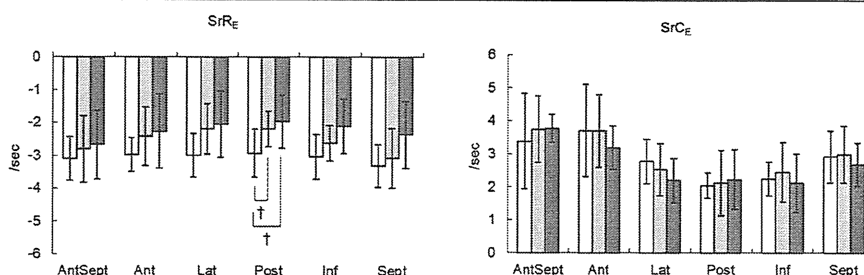

Figure 2 Segmental values of radial and circumferential strain rates during early diastole at apical and Ct levels in affected (black bars), carrier (gray bars), and normal (white bars) dogs. Data were shown as mean ± SD. †: Significant difference compared with normal dogs by multiple comparisons ($P < 0.05$). SrR_E = Peak radial strain rate during early diastole, SrC_E = Peak circumferential strain rate during early diastole, AntSept = anteroseptum, Ant = anterior, Lat = lateral, Post = posterior, Inf = inferior, Sept = septum

Table 6 Segmental values of peak radial strain rate during early diastole at Ct level in each group

Segment	Unit	Normal dogs	Carrier dogs	Affected dogs
Anterioseptum	/sec	-3.10 ± 0.66	-2.81 ± 1.01	-2.68 ± 1.05
Anterior	/sec	-2.98 ± 0.51	-2.43 ± 0.89	-2.27 ± 1.13
Lateral	/sec	-3.00 ± 0.66	-2.19 ± 0.76	-2.04 ± 1.01
Posterior	/sec	-2.93 ± 0.73	-2.19 ± 0.54†	-1.96 ± 0.81†
Inferior	/sec	-3.04 ± 0.68	-2.63 ± 0.53	-2.10 ± 0.83
Septum	/sec	-3.32 ± 0.64	-3.08 ± 0.91	-2.36 ± 1.03

†: Significant difference compared with normal dogs by multiple comparison ($P < 0.05$).

were young to middle-aged, it is possible that follow-up evaluation would reveal myocardial impairment.

In the present study, low dose of acepromazine was used for sedation. The influence of sedation was seen in EDVI, and A wave velocity of TMF. Schaefer et al. demonstrated increased A waves of TMF and myocardial velocity using TDI under anesthesia in normal mice, while increased heart rates were observed at the same time [47]. They speculated that changes in heart rates constituted one of the factors causing increased A wave velocity. Since changes in A waves in our study were accompanied by decreased heart rates, there might have been a relationship. Although further study is needed, parameters influenced by sedation appeared to be less important in the overall interpretation of our results. Additionally, proportions of sedated dogs in each group were similar.

There were several limitations in the present study. First, the number of dogs available for each group was limited and age distribution was relatively wide in all groups because of the difficulty in maintaining a sufficient number of $CXMD_J$s. Second, body weight in affected dogs was significantly lower than in normal dogs. However, we consider that this difference would be less likely to affect our results. Third, one carrier dog had mild MR. A report described mitral valve prolapse in DMD patients, and MR was considered to be responsible for LV dilation [48]. In the present study, because LV dilation was not observed in that carrier dog, MR was more likely caused by myxomatous degeneration of the mitral valve, the most common acquired heart disease in dogs. In this case, MR was considered to be too mild to likely affect our results. Fourth, the accuracy of strain measurement depends on the quality of 2-dimensional echocardiography and frame rate. The mean frame rates per cardiac cycle in normal, carrier and affected dogs were 57.4, 49.4 and 45.1, respectively. The frame rate per cardiac cycle was relatively low due to the relatively higher heart rate compared with humans (about 70-110 frames when the human heart rate was considered to be 60 bpm [49]). This may affect the accuracy of tracking quality, especially in early diastolic parameters. Further investigation using newer methods might detect change more precisely [50]. Finally, given the characteristics of this disease, differences in the sex ratio among the groups were unavoidable. Since significant differences between males and females in some STE parameters have been reported in a human study [51], the results could have been influenced by gender. Since the number of normal dogs was small when categorized by gender, further studies using a greater number of dogs are warranted. In addition, there should be some differences in expression of the disease among the affected dogs, and CXMDJ might have less severe disease compared to the human patients.

Conclusions

The myocardial strain rate by STE served to detect the impaired cardiac diastolic function in $CXMD_J$ without any obvious LV dilation or clinical signs. The radial strain rate may be a useful parameter to detect early myocardial impairment in $CXMD_J$.

List of abbreviations

LV: left ventricular; STE: speckle tracking echocardiography; CXMDJ: canine X-linked muscular dystrophy; TDI: tissue Doppler imaging; DMD: Duchenne's muscular dystrophy; Ct: chordae tendineae; LVIDd: left ventricular end-diastolic internal diameter; LVIDs: left ventricular end-systolic internal diameter; FS: fractional shortening; EF: ejection fraction; EDVI: end-diastolic volume index; ESVI: end-systolic volume index; EDV: end-diastolic volume; ESV: end-systolic volume; BSA: body surface area; LAD: left atrial diameter; AoD: aortic root diameter; LA/Ao: left atrium to aorta ratio; PEP: pre-ejection period; ET: ejection time; TMF: transmitral flow; DcT: deceleration time; IVRT: isovolumic relaxation time; MAV: mitral annulus velocity; SR: peak systolic radial strain; SC: peak systolic circumferential strain; SrR_S: peak radial strain rate during systole; SrR_E: peak radial strain rate during early diastole; SrC_S: peak circumferential strain rate during systole; SrC_E: peak circumferential strain rate during early diastole; MR: mitral regurgitation

Acknowledgements and funding

Supported by Health Sciences Research Grants for Research on Psychiatric and Neurological Diseases and Mental Health (H12-kokoro-025, H15-kokoro-021. H18-kokoro-019), Human Genome and Gene Therapy (H13-genome-001, H16-genome-003) from the Ministry of Health, Labor and Welfare of Japan, Health and Labor Sciences Research Grants for Translation Research and (H19-translational research-003) from the Ministry of Health, Labor and Welfare of Japan, Grants-in-Aid for Scientific Research from the Ministry of Education, Science, Sports and Culture of Japan (to S.T. and A.N.).

Author details

[1]Department of Surgery 1, School of Veterinary Medicine, Azabu University, Kanagawa, Japan. [2]Department of Molecular Therapy, National Institute of Neuroscience, National Center of Neurology and Psychiatry, Tokyo, Japan.

Authors' contributions

HT performed echocardiographic examinations for all dogs and statistical analysis. NY and ST contributed to hold this genetic colony of CXMDJ, and

carried out genetic examinations to determine each dog's genetic status. YF and YW conceived of the study, and participated in its design and coordination. All authors read and approved the final manuscript.

Competing interests
The authors declare that they have no competing interests.

Received: 30 September 2010 Accepted: 25 May 2011
Published: 25 May 2011

References

1. Cullen MJ, Mastaglia FL: **Morphological changes in dystrophic muscle.** *Br Med Bull* 1980, **36(2)**:145-122.
2. Nigro G, Comi LI, Politano L, Bain RJ: **The incidence and evolution of cardiomyopathy in Duchenne muscular dystrophy.** *Int J Cardiol* 1990, **26(3)**:271-277.
3. Perloff JK, de Leon AC, O'Doherty D: **The cardiomyopathy of progressive muscular dystrophy.** *Circulation* 1966, **33(4)**:625-648.
4. Danilowicz D, Rutkowski M, Myung D, Schively D: **Echocardiography in duchenne muscular dystrophy.** *Muscle Nerve* 1980, **3(4)**:298-303.
5. Farah MG, Evans EB, Vignos PJ Jr: **Echocardiographic evaluation of left ventricular function in Duchenne's muscular dystrophy.** *Am J Med* 1980, **69(2)**:248-254.
6. Hunsaker RH, Fulkerson PK, Barry FJ, Lewis RP, Leier CV, Unverferth DV: **Cardiac function in Duchenne's muscular dystrophy. Results of 10-year follow-up study and noninvasive tests.** *Am J Med* 1982, **73(2)**:235-238.
7. D'Orsogna L, O'Shea JP, Miller G: **Cardiomyopathy of Duchenne muscular dystrophy.** *Pediatr Cardiol* 1988, **9(4)**:205-213.
8. Sasaki K, Sakata K, Kachi E, Hirata S, Ishihara T, Ishikawa K: **Sequential changes in cardiac structure and function in patients with Duchenne type muscular dystrophy: a two-dimensional echocardiographic study.** *Am Heart J* 1998, **135(6 Pt 1)**:937-944.
9. Yugeta N, Urasawa N, Fujii Y, Yoshimura M, Yuasa K, Wada MR, Nakura M, Shimatsu Y, Tomohiro M, Takahashi A, Machida N, Wakao Y, Nakamura A, Takeda S: **Cardiac involvement in Beagle-based canine X-linked muscular dystrophy in Japan (CXMDJ): electrocardiographic, echocardiographic, and morphologic studies.** *BMC Cardiovasc Disord* 2006, **6**:47.
10. Yu CM, Sanderson JE, Marwick TH, Oh JK: **Tissue Doppler imaging a new prognosticator for cardiovascular diseases.** *J Am Coll Cardiol* 2007, **49(19)**:1903-1914.
11. Mori K, Edagawa T, Inoue M, Nii M, Nakagawa R, Takehara Y, Kuroda Y, Tatara K: **Peak negative myocardial velocity gradient and wall-thickening velocity during early diastole are noninvasive parameters of left ventricular diastolic function in patients with Duchenne's progressive muscular dystrophy.** *J Am Soc Echocardiogr* 2004, **17(4)**:322-329.
12. Bahler RC, Mohyuddin T, Finkelhor RS, Jacobs IB: **Contribution of Doppler tissue imaging and myocardial performance index to assessment of left ventricular function in patients with Duchenne's muscular dystrophy.** *J Am Soc Echocardiogr* 2005, **18(6)**:666-673.
13. Mori K, Hayabuchi Y, Inoue M, Suzuki M, Sakata M, Nakagawa R, Kagami S, Tatara K, Hirayama Y, Abe Y: **Myocardial strain imaging for early detection of cardiac involvement in patients with Duchenne's progressive muscular dystrophy.** *Echocardiography* 2007, **24(6)**:598-608.
14. Ogata H, Nakatani S, Ishikawa Y, Negishi A, Kobayashi M, Minami R: **Myocardial strain changes in Duchenne muscular dystrophy without overt cardiomyopathy.** *Int J Cardiol* 2007, **115(2)**:190-195.
15. Mertens L, Ganame J, Claus P, Goemans N, Thijs D, Eyskens B, Van Laere D, Bijnens B, D'Hooge J, Sutherland GR, Buyse G: **Early regional myocardial dysfunction in young patients with Duchenne muscular dystrophy.** *J Am Soc Echocardiogr* 2008, **21(9)**:1049-1054.
16. Chetboul V, Carlos C, Blot S, Thibaud JL, Escriou C, Tissier R, Retortillo JL, Pouchelon JL: **Tissue Doppler assessment of diastolic and systolic alterations of radial and longitudinal left ventricular motions in Golden Retrievers during the preclinical phase of cardiomyopathy associated with muscular dystrophy.** *Am J Vet Res* 2004, **65(10)**:1335-1341.
17. Chetboul V, Escriou C, Tessier D, Richard V, Pouchelon JL, Thibault H, Lallemand F, Thuillez C, Blot S, Derumeaux G: **Tissue Doppler imaging detects early asymptomatic myocardial abnormalities in a dog model of Duchenne's cardiomyopathy.** *Eur Heart J* 2004, **25(21)**:1934-1939.
18. Guillaume MD, Phoon CK, Chun AJ, Srichai MB: **Delayed enhancement cardiac magnetic resonance imaging in a patient with Duchenne muscular dystrophy.** *Tex Heart Inst J* 2008, **35(3)**:367-368.
19. Silva MC, Meira ZM, Gurgel Giannetti J, da Silva MM, Campos AF, Barbosa Mde M, Starling Filho GM, Ferreira Rde A, Zatz M, Rochitte CE: **Myocardial delayed enhancement by magnetic resonance imaging in patients with muscular dystrophy.** *J Am Coll Cardiol* 2007, **49(18)**:1874-1879.
20. Nishimura T, Yanagisawa A, Sakata H, Sakata K, Shimoyama K, Ishihara T, Yoshino H, Ishikawa K: **Thallium-201 single photon emission computed tomography (SPECT) in patients with duchenne's progressive muscular dystrophy: a histopathologic correlation study.** *Jpn Circ J* 2001, **65(2)**:99-105.
21. Amundsen BH, Helle-Valle T, Edvardsen T, Torp H, Crosby J, Lyseggen E, Stoylen A, Ihlen H, Lima JA, Smiseth OA, Slordahl SA: **Noninvasive myocardial strain measurement by speckle tracking echocardiography: validation against sonomicrometry and tagged magnetic resonance imaging.** *J Am Coll Cardiol* 2006, **47(4)**:789-793.
22. Becker M, Bilke E, Kuhl H, Katoh M, Kramann R, Franke A, Bucker A, Hanrath P, Hoffmann R: **Analysis of myocardial deformation based on pixel tracking in two dimensional echocardiographic images enables quantitative assessment of regional left ventricular function.** *Heart* 2006, **92(8)**:1102-1108.
23. Friedberg MK, Slorach C: **Relation between left ventricular regional radial function and radial wall motion abnormalities using two-dimensional speckle tracking in children with idiopathic dilated cardiomyopathy.** *Am J Cardiol* 2008, **102(3)**:335-339.
24. Meluzin J, Spinarova L, Hude P, Krejci J, Poloczkova H, Podrouzkova H, Pesl M, Orban M, Dusek L, Korinek J: **Left ventricular mechanics in idiopathic dilated cardiomyopathy: systolic-diastolic coupling and torsion.** *J Am Soc Echocardiogr* 2009, **22(5)**:486-493.
25. Meluzin J, Spinarova L, Hude P, Krejci J, Podrouzkova H, Pesl M, Orban M, Dusek L, Jarkovsky J, Korinek J: **Estimation of left ventricular filling pressures by speckle tracking echocardiography in patients with idiopathic dilated cardiomyopathy.** *Eur J Echocardiogr* .
26. Shimatsu Y, Yoshimura M, Yuasa K, Urasawa N, Tomohiro M, Nakura M, Tanigawa M, Nakamura A, Takeda S: **Major clinical and histopathological characteristics of canine X-linked muscular dystrophy in Japan, CXMDJ.** *Acta Myol* 2005, **24(2)**:145-154.
27. Shimatsu Y, Katagiri K, Furuta T, Nakura M, Tanioka Y, Yuasa K, Tomohiro M, Kornegay JN, Nonaka I, Takeda S: **Canine X-linked muscular dystrophy in Japan (CXMDJ).** *Exp Anim* 2003, **52(2)**:93-97.
28. Urasawa N, Wada MR, Machida N, Yuasa K, Shimatsu Y, Wakao Y, Yuasa S, Sano T, Nonaka I, Nakamura A, Takeda S: **Selective vacuolar degeneration in dystrophin-deficient canine Purkinje fibers despite preservation of dystrophin-associated proteins with overexpression of Dp71.** *Circulation* 2008, **117(19)**:2437-2448.
29. Jacobs G, Mahjoob K: **Multiple regression analysis, using body size and cardiac cycle length, in predicting echocardiographic variables in dogs.** *Am J Vet Res* 1988, **49(8)**:1290-1294.
30. Rishniw M, Erb HN: **Evaluation of four 2-dimensional echocardiographic methods of assessing left atrial size in dogs.** *J Vet Intern Med* 2000, **14(4)**:429-435.
31. Atkins CE, Snyder PS: **Systolic time intervals and their derivatives for evaluation of cardiac function.** *J Vet Intern Med* 1992, **6(2)**:55-63.
32. Chetboul V, Sampedrano CC, Concordet D, Tissier R, Lamour T, Ginesta J, Gouni V, Nicolle AP, Pouchelon JL, Lefebvre HP: **Use of quantitative two-dimensional color tissue Doppler imaging for assessment of left ventricular radial and longitudinal myocardial velocities in dogs.** *Am J Vet Res* 2005, **66(6)**:953-961.
33. Oyama MA, Sisson DD, Bulmer BJ, Constable PD: **Echocardiographic estimation of mean left atrial pressure in a canine model of acute mitral valve insufficiency.** *J Vet Intern Med* 2004, **18(5)**:667-672.
34. Kim HK, Sohn DW, Lee SE, Choi SY, Park JS, Kim YJ, Oh BH, Park YB, Choi YS: **Assessment of left ventricular rotation and torsion with two-dimensional speckle tracking echocardiography.** *J Am Soc Echocardiogr* 2007, **20(1)**:45-53.
35. Chetboul V, Serres F, Gouni V, Tissier R, Pouchelon JL: **Noninvasive assessment of systolic left ventricular torsion by 2-dimensional speckle tracking imaging in the awake dog: repeatability, reproducibility, and comparison with tissue Doppler imaging variables.** *J Vet Intern Med* 2008, **22(2)**:342-350.

36. Suffoletto MS, Dohi K, Cannesson M, Saba S, Gorcsan J III: **Novel speckle-tracking radial strain from routine black-and-white echocardiographic images to quantify dyssynchrony and predict response to cardiac resynchronization therapy.** *Circulation* 2006, **113(7)**:960-968.
37. Takano H, Fujii Y, Ishikawa R, Aoki T, Wakao Y: **Comparison of left ventricular contraction profiles among small, medium, and large dogs by use of two-dimensional speckle-tracking echocardiography.** *Am J Vet Res* **71(4)**:421-427.
38. Park TH, Nagueh SF, Khoury DS, Kopelen HA, Akrivakis S, Nasser K, Ren G, Frangogiannis NG: **Impact of myocardial structure and function postinfarction on diastolic strain measurements: implications for assessment of myocardial viability.** *Am J Physiol Heart Circ Physiol* 2006, **290(2)**:H724-731.
39. Wang J, Khoury DS, Thohan V, Torre-Amione G, Nagueh SF: **Global diastolic strain rate for the assessment of left ventricular relaxation and filling pressures.** *Circulation* 2007, **115(11)**:1376-1383.
40. Moriuchi T, Kagawa N, Mukoyama M, Hizawa K: **Autopsy analyses of the muscular dystrophies.** *Tokushima J Exp Med* 1993, **40(1-2)**:83-93.
41. Frankel KA, Rosser RJ: **The pathology of the heart in progressive muscular dystrophy: epimyocardial fibrosis.** *Hum Pathol* 1976, **7(4)**:375-386.
42. Mori K, Manabe T, Nii M, Hayabuchi Y, Kuroda Y, Tatara K: **Myocardial integrated ultrasound backscatter in patients with Duchenne's progressive muscular dystrophy.** *Heart* 2001, **86(3)**:341-342.
43. O'Sullivan ML, O'Grady MR, Minors SL: **Assessment of diastolic function by Doppler echocardiography in normal Doberman Pinschers and Doberman Pinschers with dilated cardiomyopathy.** *J Vet Intern Med* 2007, **21(1)**:81-91.
44. Nagueh SF, Appleton CP, Gillebert TC, Marino PN, Oh JK, Smiseth OA, Waggoner AD, Flachskampf FA, Pellikka PA, Evangelisa A: **Recommendations for the evaluation of left ventricular diastolic function by echocardiography.** *Eur J Echocardiogr* 2009, **10(2)**:165-193.
45. Ueda Y, Kawai H, Adachi K, Naruo T, Saito S: **Cardiac dysfunction in female gene carriers of Duchenne muscular dystrophy.** *Rinsho Shinkeigaku* 1995, **35(11)**:1191-1198.
46. Mirabella M, Servidei S, Manfredi G, Ricci E, Frustaci A, Bertini E, Rana M, Tonali P: **Cardiomyopathy may be the only clinical manifestation in female carriers of Duchenne muscular dystrophy.** *Neurology* 1993, **43(11)**:2342-2345.
47. Schaefer A, Meyer GP, Brand B, Hilfiker-Kleiner D, Drexler H, Klein G: **Effects of anesthesia on diastolic function in mice assessed by echocardiography.** *Echocardiography* 2005, **22(8)**:665-670.
48. Sanyal SK, Johnson WW, Dische MR, Pitner SE, Beard C: **Dystrophic degeneration of papillary muscle and ventricular myocardium. A basis for mitral valve prolapse in Duchenne's muscular dystrophy.** *Circulation* 1980, **62(2)**:430-438.
49. Helle-Valle T, Crosby J, Edvardsen T, Lyseggen E, Amundsen BH, Smith HJ, Rosen BD, Lima JA, Torp H, Ihlen H, Smiseth OA: **New noninvasive method for assessment of left ventricular rotation: speckle tracking echocardiography.** *Circulation* 2005, **112(20)**:3149-3156.
50. Tournoux F, Chan RC, Handschumacher MD, Salgo IS, Manzke R, Settlemier S, Guerrero JL, Cury RC, Weyman AE, Picard MH: **Estimation of radial strain and rotation using a new algorithm based on speckle tracking.** *J Am Soc Echocardiogr* 2008, **21(10)**:1168-1174.
51. Hurlburt HM, Aurigemma GP, Hill JC, Narayanan A, Gaasch WH, Vinch CS, Meyer TE, Tighe DA: **Direct ultrasound measurement of longitudinal, circumferential, and radial strain using 2-dimensional strain imaging in normal adults.** *Echocardiography* 2007, **24(7)**:723-731.

Pre-publication history
The pre-publication history for this paper can be accessed here:
http://www.biomedcentral.com/1471-2261/11/23/prepub

doi:10.1186/1471-2261-11-23
Cite this article as: Takano *et al.*: Assessment of left ventricular regional function in affected and carrier dogs with duchenne muscular dystrophy using speckle tracking echocardiography. *BMC Cardiovascular Disorders* 2011 11:23.

Submit your next manuscript to BioMed Central and take full advantage of:

- Convenient online submission
- Thorough peer review
- No space constraints or color figure charges
- Immediate publication on acceptance
- Inclusion in PubMed, CAS, Scopus and Google Scholar
- Research which is freely available for redistribution

Submit your manuscript at
www.biomedcentral.com/submit

JOC The Journal of Organic Chemistry

ARTICLE

pubs.acs.org/joc

Synthesis of 2′-O-[2-(N-Methylcarbamoyl)ethyl]ribonucleosides Using Oxa-Michael Reaction and Chemical and Biological Properties of Oligonucleotide Derivatives Incorporating These Modified Ribonucleosides

Takeshi Yamada,[†] Natsuki Okaniwa,[†] Hisao Saneyoshi,[†] Akihiro Ohkubo,[†] Kohji Seio,[†] Tetsuya Nagata,[‡] Yoshitsugu Aoki,[‡] Shin'ichi Takeda,[‡] and Mitsuo Sekine*[,†]

[†]Department of Life Science, Tokyo Institute of Technology, J2-12, 4259 Nagatsuta, Midoriku, Yokohama 226-8501, Japan

[‡]Department of Molecular Therapy, Institute of Neuroscience, National Center of Neurology and Psychiatry, 4-1-1 Ogawa-Higashi, Kodaira, Tokyo 187-8502, Japan

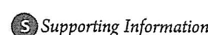

Supporting Information

ABSTRACT: To develop oligonucleotides containing new 2′-O-modified ribonucleosides as nucleic acid drugs, we synthesized three types of ribonucleoside derivatives modified at the 2′-hydroxyl group with 2-(methoxycarbonyl)ethyl (MOCE), 2-(N-methylcarbamoyl)ethyl (MCE), and 2-(N,N-dimethylcarbamoyl)ethyl (DMCE) groups, as key intermediates, via the oxa-Michael reaction of the appropriately protected ribonucleoside (U, C, A, and G) derivatives. Among them, the 2′-O-MCE ribonucleosides were found to be the most stable under basic conditions. To study the effects of the 2′-O-modification on the nuclease resistance of oligonucleotides incorporating the 2′-O-modified ribonucleosides and their hybridization affinities for the complementary RNA and DNA strands, 2′-O-MCE-ribonucleoside phosphoramidite derivatives were successfully synthesized and subjected to the synthesis of 2′-O-MCE-oligonucleotides and 2′-O-methyl-oligonucleotides incorporating 2′-O-MCE-ribonucleosides. The 2′-O-MCE-oligonucleotides and chimeric oligomers with 2′-O-MCE and 2′-O-methyl groups thus obtained demonstrated complementary RNA strands and much higher nuclease resistances than the corresponding 2′-O-methylated species. Finally, we incorporated the 2′-O-MCE-ribonucleosides into antisense 2′-O-methyl-oligoribonucleotides to examine their exon-skipping activities in splicing reactions related to pre-mRNA of mouse dystrophin. The exon-skipping assay of these 2′-O-methyl-oligonucleotide incorporating 2′-O-MCE-uridines showed better efficacies than the corresponding 2′-O-methylated oligoribonucleotide phosphorothioate derivatives.

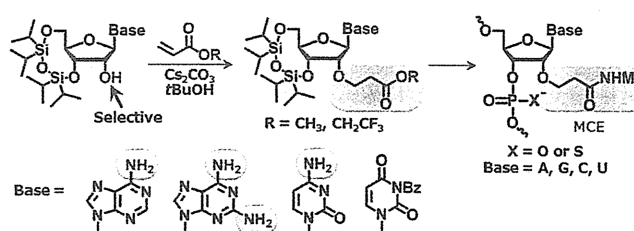

INTRODUCTION

A number of 2′-O-modified ribonucleosides have been designed and synthesized for oligonucleotide-based therapeutics, represented by the silencing of mRNAs using siRNAs,[1] antisense RNAs,[2] and shRNAs[3] and the suppression of specific proteins using RNA aptamers.[4] Various modifications with substituent groups, such as 2′-O-methyl,[5] 2′-O-methoxyethyl,[6] 2′-O-aminopropyl,[7] and 2′-O-[2-(methylamino)-2-oxoethyl],[8] have been reported to date. The incorporation of these 2′-O-modified nucleosides into oligoribonucleotides has proven to be useful for improving their stability against hydrolysis by nucleases in serum,[9] controlling their biodistribution in cells and organs,[10] and enhancing their hybridization affinities for the complementary RNAs.[11] 2′-O-Modification of ribonucleosides was also used for the introduction of tethers with other small molecules such as lipids,[12] dyes,[13] and peptides.[14] Several 2′-O-modified ribonucleoside derivatives have been synthesized via the ring-opening reaction of 2,2′-anhydrouridine[15] and the alkylation of appropriately protected ribonucleosides with alkyl halides under strong basic conditions.[16] Meanwhile, we independently reported the synthesis and properties of 2′-O-cyanoethyl-modified (2′-O-CE) oligonucleotides[17] (Figure 1). 2′-O-CE oligoribonucleotides demonstrated higher hybridization affinities for the cDNAs and RNAs than the corresponding unmodified species; they also demonstrated favorable nuclease resistances. These results indicated that 2′-O-CE oligonucleotides would be available for oligonucleotide therapy; however, they were somewhat unstable under basic conditions. The 2′-O-CE group was gradually removed via β-elimination under basic conditions such as aqueous ammonia. We also found that the CE group could be used as a protecting group of 2′-OH in RNA synthesis, since this group could be removed by treatment with 1 M Bu_4NF in THF.[18]

On the basis of the previous results, we designed three types of ribonucleosides modified at the 2′-hydroxyl group with 2-(methoxycarbonyl)ethyl (MOCE) (**1**), 2-(N-methylcarbamoyl)ethyl (MCE) (**2**), and 2-[(N,N-dimethylcarbamoyl)ethyl

Received: October 5, 2010
Published: March 23, 2011

ACS Publications © 2011 American Chemical Society

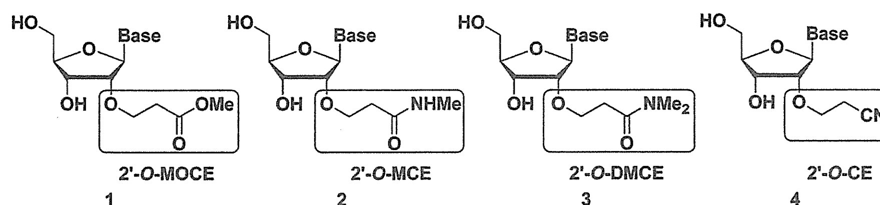

Figure 1. The structures of 2′-O-MOCE, 2′-O-MCE, 2′-O-DMCE, and 2′-O-CE ribonucleosides.

(DMCE) (3) groups as novel monomer components of 2′-O-modified oligoribonucleotides, as shown in Figure 1. We expected that these modifiers could be introduced via Michael additions similar to the $CsCO_3$-mediated 2′-O-cyanoethylation used for the synthesis of 2′-O-CE ribonucleosides (4) followed by amidation. It seemed that the transformation of the cyano group in the CE group to weaker electron-withdrawing groups, such as methoxycarbonyl, N-methylcarbamoyl, and N,N-dimethylcarbamoyl, could suppress the loss of these 2′-O-modifiers due to β-elimination during the entire synthetic process involving ammonia treatment required for removal of base-protecting groups. The MCE and DMCE groups have amide functions in their structures. Prakash et al. previously reported that oligoribonucleotides incorporating 2′-O-[2-(methylamino)-2-oxoethyl]ribonucleosides with an amide group similar to that of 2′-O-MCE ribonucleosides showed favorable nuclease resistance.[9]

In this paper, we report the details of the synthesis of new 2′-O-modified ribonucleosides, which involved highly selective oxa-Michael additions for purine nucleotides without alkylation of the base residues, such as cytosine, adenine, and 2-aminoadenine, and several unique properties of oligonucleotide derivatives incorporating these 2′-O-modified ribonucleosides. In addition to these synthetic studies, promising biological properties of 2′-O-MCE/2′-O-Me chimeric RNA oligomers, involving an effective exon skipping of the pre-mRNA of mouse dystrophin, are also described.

RESULTS AND DISCUSSION

Oxa-Michael Addition of the Secondary 2′-O-Hydroxyl Group of Uridine to Acrylates. We tested various α,β-unsaturated carbonyl compounds, such as alkyl acrylates ($CH_2{=}CHC(O)OR$: R = CH_3, C_2H_5, n-C_4H_9, t-C_4H_9, and CF_3CH_2), acrylamide, N,N-dimethylacrylamide, acrolein, and methyl vinyl ketone, as the acceptors of the oxa-Michael addition of N^3-benzoyl-3′,5′-O-(1,1,3,3-tetraisopropyldisiloxane-1,3-diyl)uridine (5)[19] in t-BuOH in the presence of cesium carbonate at room temperature for 2−18 h, as shown in Scheme 1. Before compound 5 was selected for the Michael addition donor, 3′,5′-O-(1,1,3,3-tetraisopropyldisiloxane-1,3-diyl)uridine[20] was tested. However, the alkylation reaction on the uridine moiety was faster than Michael addition to the 2′-hydroxyl group. When methyl, ethyl, and 2,2,2-trifluoroethyl esters of acrylic acid were used, the oxa-Michael reactions proceeded smoothly to give 2′-O-alkylated compounds 6, 7, and 8, respectively. Other acceptors, such as n-butyl acrylates, tert-butyl alkylate, acrylamide, N,N-dimethylacrylamide, acrolein, and methyl vinyl ketone, were ineffective under these conditions. The reaction rate increased by increasing the substrate concentration from 0.1 to 0.2 M. The polymerization of the Michael acceptors did not occur in most cases, except for the reaction of 5 with acrolein.

Scheme 1. Oxa-Michael Reaction to Compound 5[a]

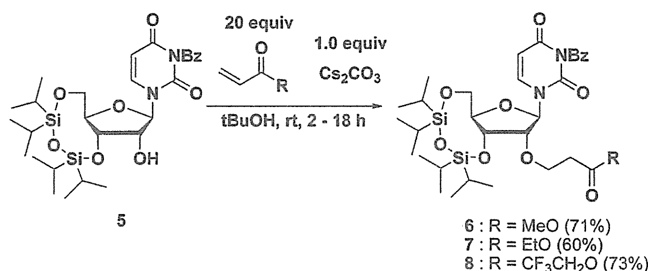

[a] Conditions: acrylate ester derivatives, Cs_2CO_3, t-BuOH, rt, 2−18 h; yield: 6 (71%), 7 (60%), 8 (73%).

Functional Group Transformation of 2′-O-[2-(Alkoxycarbonyl)ethyl]uridine. Scheme 2 shows the synthesis of 5′-O-(4,4′-dimethoxytrityl)uridine derivatives modified at the 2′-position with MOCE, MCE, and DMCE groups. The benzoyl group of the methyl ester compound 6 was selectively removed by treatment with 5 equiv of n-$PrNH_2$ in THF to give the deprotetected compound 9. The methyl ester group was inert under these conditions. When compound 6 was treated with 40% $MeNH_2$ in MeOH, the monoalkyl amide 10 was obtained in a good yield. However, treatment of compound 6 with 2 M Me_2NH in THF did not give the desired dialkyl amide 11 but instead gave the debenzoylated compound 9 quantitatively. The use of 50% Me_2NH in H_2O resulted in the formation of a hydrolyzed compound as the main product (data not shown). Therefore, we chose the more reactive ester 8 for the synthesis of 11. As a result, treatment of compound 8 with 2 M Me_2NH in THF easily gave compound 11. Treatment of compounds 9−11 with $Et_3N\cdot 3HF$ gave the resulting 3′,5′-unprotected intermediates 12−14, which were allowed to react with DMTrCl to give compounds 15−17, respectively.

Chemical Properties of the MOCE, MCE, and DMCE Groups of 15−17 under Basic Conditions. We investigated the stability of the MOCE, MCE, and DMCE groups of 15−17 under basic conditions; Table 1 summarizes these results. We treated 10 mg of each compound with 1 mL of 1 M NaOH, 28% NH_4OH, and 1 M TBAF in THF, and checked the time course of the reaction by silica gel thin layer chromatography analysis.

Treatment with 1 M NaOH easily hydrolyzed the methyl ester 15 to give the carboxylic acid 18 in 65% yield. The ammonia treatment of compound 15 also resulted in rapid ammonolysis, giving rise to the amide compound 19. These results showed that hydrolysis and ammonolysis were much faster than β-elimination, and once the ester was transformed to the amide or the carboxylic acid, further β-elimination was well suppressed. We isolated and identified the hydrolyzed product 18 and the amidate derivative 19 by ^{1}H NMR and HRMS. Rapid removal of the MOCE group took place when compound 15 was treated